



The exposed Mule Creek vent deposits record the structure of a volcanic conduit during a hybrid explosive–effusive eruption

Holly E. Unwin¹ · Hugh Tuffen¹ · Fabian B. Wadsworth² · Emrys R. Phillips³ · Mike R. James¹ · Annabelle Foster² · Stephan Kolzenburg⁴ · Jonathan M. Castro⁵ · Lucy A. Porritt⁶

Received: 20 May 2022 / Accepted: 18 March 2023 / Published online: 4 April 2023
© The Author(s) 2023

Abstract

Silicic volcanic eruptions commonly begin with the explosive ejection of pyroclastic material, before transitioning to gentler effusion-dominated activity. Well-exposed dissected silicic systems are scarce and poorly studied, hindering the advances in our understanding of the explosive–effusive transition needed to improve interpretations of volcanic unrest and hazard forecasting. The Mule Creek vent (New Mexico, USA) is a dissected silicic conduit that records the processes controlling conduit formation and evolution, and the role tuffisites (fractures filled with variably welded pyroclasts) play in conduit dynamics. Here, we use decimeter-scale photo-mapping of lithostratigraphic units and thin section analysis to differentiate and interpret three dominant emplacement styles during vent evolution. First, there was repeated deposition and erosion of pyroclastic material at the conduit walls, recorded by erosive surfaces in pyroclastic breccia and agglomerates at the conduit margins. Second, sub-vertical domains of dense melt-dominated magma were emplaced and preserved as glass-dominated vitrophyre and brecciated vitrophyre, with the textural hallmarks of assembly from welding of pyroclasts. Finally, the sub-horizontal fracturing of previously deposited lithologies produced laterally cross-cutting tuffisites. The vent deposits track the widening and then narrowing of the conduit through time and reflect progressive insulation and generally higher temperatures towards the conduit center as pyroclasts accumulate. Welding of pyroclastic fill and the formation of dense vitrophyres towards the conduit center lowers deposit porosity and effective wall permeability. This drives localized gas pressure increases and results in gas-driven fracturing, generating tuffisites, which act as transient outgassing pathways. The structure of the Mule Creek vent records an explosive–effusive transition, constraining the processes controlling conduit evolution and aiding our interpretation of volcanic unrest.

Keywords Tuffisite · Hydrofracture · Rhyolite · Volcanic degassing · Conduit

Introduction

Silicic volcanic eruptions are preceded by the opening of fractures driven by high-pressure gas–ash mixtures (McGowan 2016), often in fissures (Lara 2009). These fissures then localize to single vents (Schipper et al. 2013). The first pyroclastic deposits recording this opening phase of explosive eruptions typically involve a high proportion of lithics, diagnostic of country rock fracturing, and vent-clearing and widening (e.g., Stasiuk et al. 1996; Campbell et al. 2013; Schipper et al. 2013). The volcanic conduit is the ascent pathway along which material is transported towards the surface, and the vent is the uppermost part of this conduit system, which often flares as it approaches within ~300–500 m of the surface (Wilson & Head 1981; Cataldo et al. 2013). In silicic systems, the eruption onset is often characterized

Editorial Responsibility: N. Pardo

✉ Holly E. Unwin
h.unwin@lancaster.ac.uk

¹ Lancaster Environment Centre, Lancaster University, Lancaster, UK

² Department of Earth Sciences, Durham University, Durham, UK

³ British Geological Survey, The Lyell Centre, Edinburgh, UK

⁴ Department of Geology, University at Buffalo, New York, USA

⁵ Institute of Geosciences, Johannes Gutenberg University Mainz, Mainz, Germany

⁶ Department of Earth, Ocean and Atmospheric Sciences, University of British Columbia, Vancouver, Canada

by high-energy explosive activity (Cassidy et al. 2018) involving the eruption of gas and pyroclastic material, before transitioning to effusive activity dominated by the comparatively gentle eruption of lava (Eichelberger et al. 1986). The switch between explosive and effusive activity is thought to broadly represent a transition from closed system degassing to more open-system outgassing, where gas can escape from the magma and the conduit system, releasing gas pressure (Eichelberger et al. 1986; Jaupart & Allègre 1991).

Open-system outgassing may occur vertically or laterally, with lateral outgassing allowing gas to escape from the magma and flow through permeable conduit margins, either through permeable host rock (Jaupart & Allègre 1991; Rust et al. 2004; Lavallée et al. 2013; Farquharson et al. 2015; Kolzenburg et al. 2019), permeable tephra-lined conduit margins (Rust et al. 2004) or permeable particle filled fractures—known as external tuffisites—created by the injection of ash–gas mixtures into fractures within the conduit walls (Cloos 1941; Heiken et al. 1988; Goto et al. 2008; Unwin et al. 2021). In contrast, open-system vertical outgassing requires either long-range magma permeability (e.g., an extensive magmatic foam), long-range fractures (such as internal tuffisites), a compacting column of fragmental material within the vent (Kolzenburg & Russell 2014), or dynamic outgassing during fragmentation and explosive eruption, before welding (Wadsworth et al. 2020). Internal tuffisites have been proposed to form in hot magma within a volcanic conduit when shear stresses reach or exceed the strength of the magma, forming interconnected fracture networks (Kendrick et al. 2016; Saubin et al. 2016). Tuffisites in magma have been touted as permeable outgassing pathways, potentially allowing sufficient outgassing to moderate eruption explosivity (Jaupart 1998; Castro et al. 2012, 2014; Berlo et al. 2013; Farquharson et al. 2017; Heap et al. 2019; Kolzenburg et al. 2019). However, tuffisite permeability is only transient as welding progressively destroys pore space between hot fracture-propping particles (Stasiuk et al. 1996; Tuffen et al. 2003; Heap et al. 2019; Kolzenburg et al. 2019; Wadsworth et al. 2021).

Direct observations of silicic eruptive activity at Volcán Chaitén (2008–2009) and Cordón Caulle (2011–2012), both in Chile, show that the effusive eruption of silicic lava is interrupted by intermittent explosions (hybrid activity), with gas and ash erupted through fractures in the vent-filling lava itself (Castro & Dingwell 2009; Schipper et al. 2013). The recognition that fragmented material trapped in lava-hosted fractures can weld to produce a continuous melt by viscous sintering (Gardner et al. 2018, 2019; Wadsworth et al. 2019, 2021; Farquharson et al. 2022), and the discovery of obsidian clasts and bombs formed of welded fragments (Cabrera et al. 2015; Gardner et al. 2017; Giachetti et al. 2021; Schipper et al. 2021), has led to models suggesting that the accretion of clastic material on to the conduit walls could form both

obsidian pyroclasts (Gardner et al. 2017, 2019) and silicic lava (Wadsworth et al. 2020, 2022). Simultaneous explosive and effusive activity has been explained by continued fragmentation at depth, with effusive lava formed by either material accreting and welding at the conduit walls (Wadsworth et al. 2020), or a rising column of intact and degassing magma that does not fill the entire conduit (Schipper et al. 2021).

Dissected mafic systems, such as diatremes, are more common and better studied than silicic vents (e.g., White & Ross 2011; Valentine & White 2012; Ross et al. 2017). Diatremes and silicic vents share many similarities, with both formed of an inverse cone-shaped body of pyroclastic material created by blasting and then deposition, and a complex internal structure formed by the continued overturning of previously deposited material (e.g., Ross & White 2006; Schipper et al. 2021; Valentine & Cole 2021; Wadsworth et al. 2022). Comparing and contrasting these systems would help to improve our understanding of both groups. Dissected silicic vents provide an opportunity to examine structures and textures of an upper conduit system and test the diverse hypotheses for vent processes described above. The Mule Creek vent, New Mexico (USA), is a classic example of a dissected silicic vent and is a type locality for examining the relationships between tuffisites and the vent that they intersect (Fig. 1a and b; Stasiuk et al. 1996). Many features of the Mule Creek vent are described in detail by Stasiuk et al. (1996). Here, we build on their observations, focusing on a large outcrop of pyroclastic breccia at the vent margin that provides new insights into the early stages of vent evolution.

Geological setting of the Mule Creek vent

The Mule Creek vent (MCV) is located ~8 km north of Mule Creek in the Gila National Forest, southwestern New Mexico, USA (Fig. 1a), and is the best exposed of at least six genetically linked rhyolitic plugs and vents distributed along the northwest trending Potholes Country Graben (Stasiuk et al. 1996; Ratté 2004), together with voluminous pyroclastic deposits. The MCV was formed during an eruption emplacing the 20–21 Ma Potholes Country rhyolite, a lava flow which is mostly confined within the Potholes Country Graben (Stasiuk et al. 1996). The Mule Creek vent is exposed in a tall canyon 350 m deep, cutting through the ~23–25 Ma Bearwallow Mountain andesite host rock (Fig. 1b). The flared shape of the vent towards the canyon rim suggests that the canyon exposes the uppermost ~350 m of the vent. The upper half of the canyon is encased in bedded rhyolitic tephra up to 150 m thick, emplaced during vent formation, indicating the position of the palaeosurface before the formation of the MCV (Fig. 2a and b; Ratté 2004). The Bearwallow Mountain andesite at the canyon base is composed of vesicular brecciated andesite lavas that are red brown to grey in color. The pyroclastic deposits are

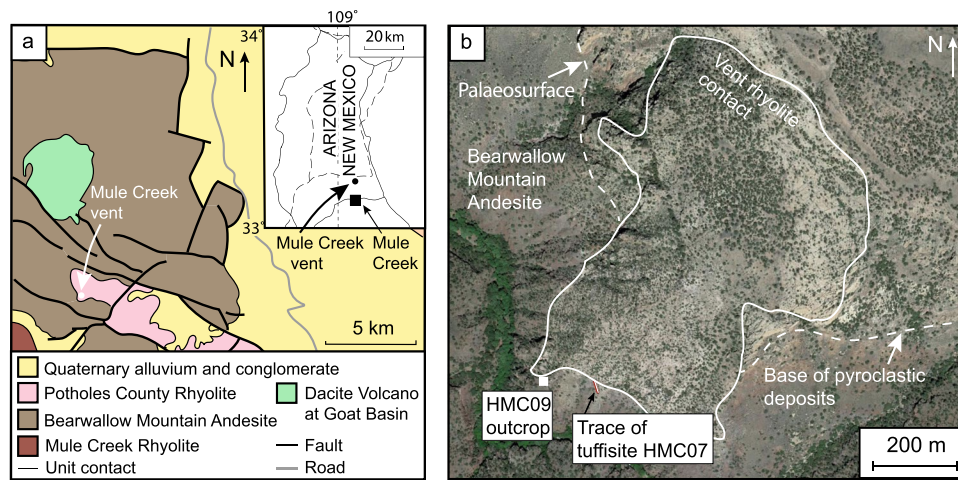
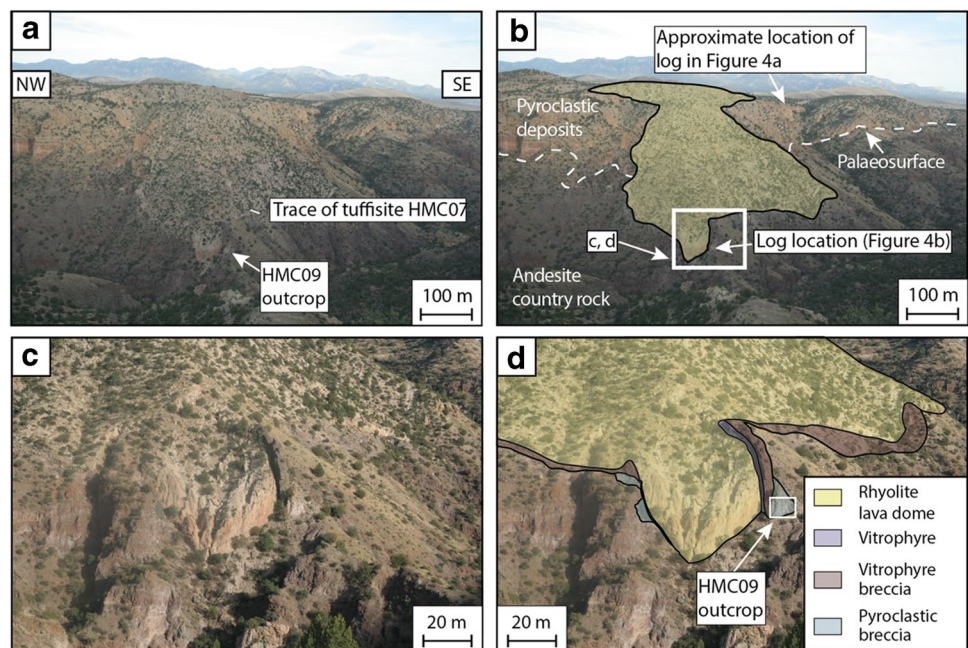


Fig. 1 **a** Location and geological setting of the Mule Creek, vent 8 km north of Mule Creek, Gila National Forest, New Mexico, USA; modified from Stasiuk et al. (1996) and Ratté et al. (2004). The geological map indicates the position of the Mule Creek Vent within the

northwest trending Potholes County graben. **b** Map view of the Mule Creek vent with the vent rhyolite lava contact, base of the pyroclastic deposit and sample locations marked. Map imagery: Google, ©2022 Maxar Technologies, NMRGIS, USDA Farm Service Agency

Fig. 2 Overview photographs of the Mule Creek vent. **a** Overview photograph showing the field location, taken looking NE. **b** The same view as in part a but with a simplified geological interpretation overlain. **c** A zoomed-in photograph showing the structure of the vent more clearly. **d** The same view as in part c but with a simplified geological interpretation overlain. Outcrop names and key features are marked



sub-horizontally bedded > 100 m from the vent, and their dip into the vent increases closer to the contact with the Potholes Country rhyolite lava (Stasiuk et al. 1996).

Field and analytical methods

A large outcrop of pyroclastic breccia at the vent margin was identified during fieldwork at the MCV in 2010 (HMC09, Figs. 1b and 2), with a greater thickness and more complex internal structure than that described by Stasiuk et al. (1996).

Samples and photographs of the MCV units and intersecting tuffsites were collected, enabling the multiscale (macro and micro) analysis of the four different vent units (pyroclastic breccia, vitrophyre breccia, vitrophyre, and central rhyolite lava) and their intersecting tuffsites. Thin sections were prepared from a sub-set of the hand specimens and have been used as part of a detailed microstructural study. In addition, polished thin sections were examined using a Hitachi SU-70 high-resolution scanning electron microscope with a 15 kV beam voltage and 15 mm working distance. Backscattered electron (BSE) images of the tuffsite matrix

were taken of all samples at an appropriate scale to capture ~200 grains in each image for particle size distributions, with the collected images each 1280×960 pixels. The area of the pyroclastic breccia imaged to produce the particle size distribution was 0.016 mm^2 at $\times 800$ magnification with a scale of $17.5 \text{ pixels}/\mu\text{m}$. The area of vitrophyre breccia imaged was 0.1 mm^2 at $\times 300$ magnification with a scale of $3.0 \text{ pixels}/\mu\text{m}$.

Particle size distributions for particles within tuffisites were determined by measuring the area of particles in back-scattered electron images using ImageJ (Schneider et al. 2012). The low contrast between particles and their touching margins prevented effective image thresholding for particle detection (Lormand et al. 2018). Therefore, the margins of each particle were traced manually. The traced particles were then separated out and each particle measured individually using ImageJ. The particle area data collected reflects 2D slices through 3D samples in the thin section but will here be referred to as particle size for simplicity.

The particle area was converted to an equivalent diameter for each particle using $d = \sqrt{4A/\pi}$, where A is the measured particle area and d is the equivalent spherical particle diameter. The circularity of the average particle in each image ranged from ~0.74 to 0.85, calculated with the in-built algorithm within ImageJ (imagej.nih.gov/ij/; Schneider et al. 2012). Any particle with an equivalent diameter less than 10 pixels across or an area greater than 1% of the measured image area were considered not to be sufficiently well represented in the data and were filtered out (Shea et al. 2010). The particles were sorted into a series of geometric bins, with the smallest bin equal to the minimum size threshold (10 pixels in diameter) and each subsequent bin $10^{0.1}$ larger than the previous. The histogram was then normalized so that the sum of the areas is equal to one, converting to particle area fraction.

Field observations

The MCV is composed of a series of four major vent units, with the outermost unit comprising a pyroclastic breccia in contact with the andesite country rock (Figs. 2c and d and 3; Stasiuk et al. 1996). The pyroclastic breccia is bordered on the inside edge by two dark-colored units with a glassy appearance (i.e., nominally aphyric albeit with some microlite-dominated flow bands), termed by Stasiuk et al. (1996) as a vitrophyre breccia and a vitrophyre. The vitrophyre breccia is composed of heavily fractured clasts of glassy material and borders the pyroclastic breccia. The vitrophyre breccia becomes less heavily fractured and more sheared towards the center to form a vitrophyre unit formed of more coherent glass (Figs. 3a and b). The vitrophyre unit grades into a flow-banded rhyolite lava at the vent center

(Stasiuk et al. 1996). The vent units are intersected by particle-filled fractures known as tuffisite veins, which form either steeply dipping and aligned features or sub-horizontal structures (Figs. 3a and b). Tuffisites injected into the walls of the MCV are defined as external tuffisites and may be constrained to an individual vent unit or in some cases cross-cut multiple vent units. These external tuffisite veins are filled with fragments of their host rock, as well as ash-sized particles that preserve sedimentary structures such as laminations.

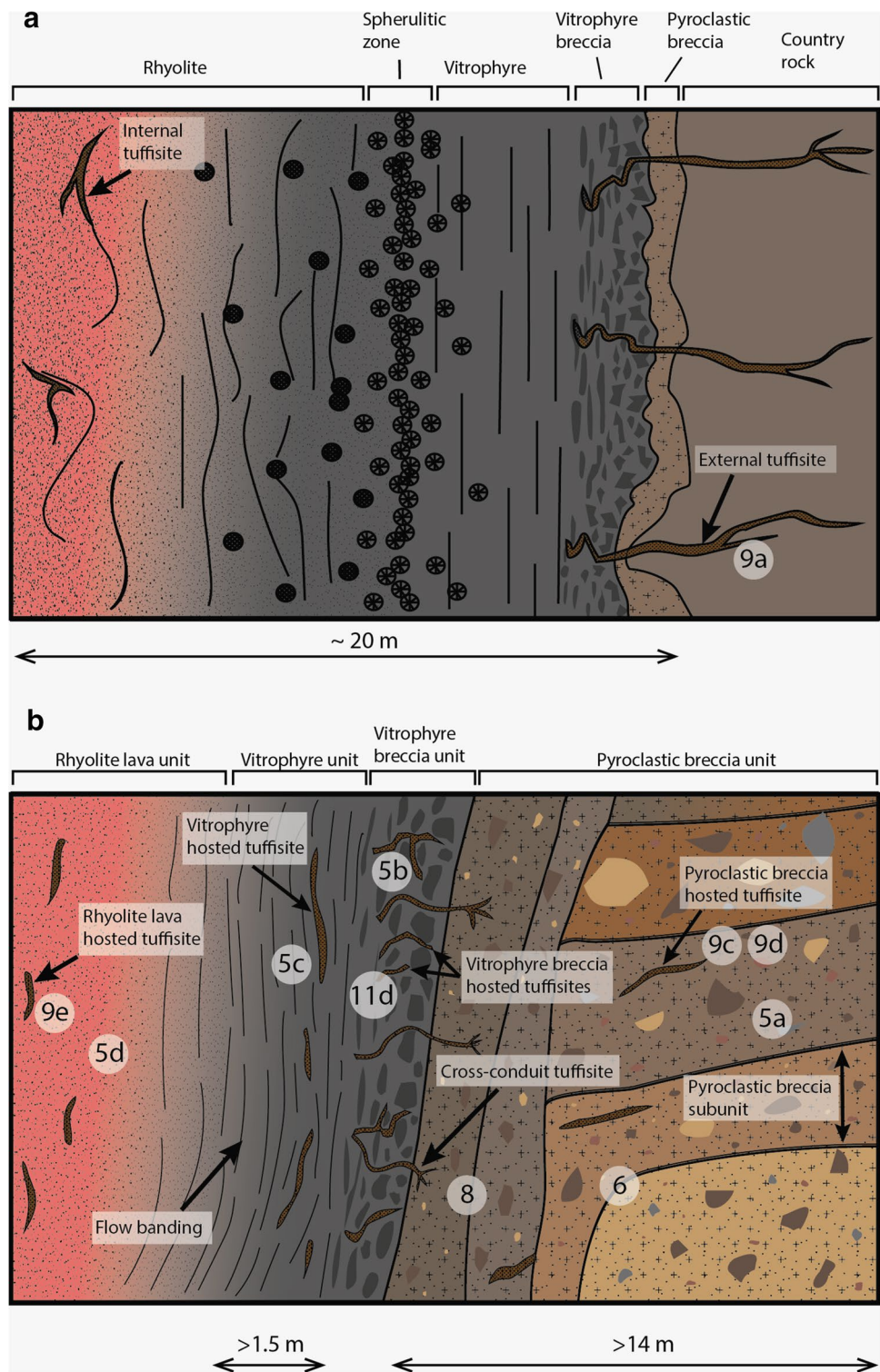
The following sections describe field and sample observations that augment and supplement those described by Stasiuk et al. (1996). We report observations on a locality down-slope (~250 m deeper) from those investigated by Stasiuk et al. (1996), focusing on the pyroclastic breccia, vitrophyre breccia and vitrophyre units, and tuffisites (HMC09; Figs. 2c and d).

Pyroclastic breccia and apron

Pyroclastic deposits around the vent form a ≤ 150 m thick apron (Fig. 1b; Stasiuk et al. 1996), with subunits closer to the rhyolite lava contact dipping more steeply ($\leq 20^\circ$) into the vent than those further away (Fig. 3b) and commonly showing evidence of gravitational slumping. At distances > 100 m from the rhyolite lava contact, the pyroclastic deposits are approximately sub-horizontally stratified or dip away from the vent ($\leq 5^\circ$). A transect through this pyroclastic apron at the canyon rim reveals that they become relatively less lithic-rich (fewer non-juvenile clasts) and increasingly pumice-dominated moving stratigraphically up-section (Fig. 4a; Stasiuk et al. 1996).

The outermost unit of the MCV is a pyroclastic breccia that is in contact with either the pyroclastic apron or the Bearwallow Mountain andesite country rock (Stasiuk et al. 1996). Clasts in the pyroclastic breccia are composed of rounded pumice and angular lithic fragments derived from the Bearwallow Mountain andesite (Fig. 5a). Close to the canyon rim, Stasiuk et al. (1996) recorded the pyroclastic breccia as being 0.2–2 m thick and infilling irregularities at the vent margin. This study focuses on the characteristics of a much thicker (> 14 m) pyroclastic breccia sequence exposed closer to the base of the canyon on the eastern side of the vent (HMC09, Figs. 2a and d and 6). This outcrop is ~100 m deeper than the base of pyroclastic apron mapped by Stasiuk et al. (1996), which can be seen in satellite imagery and field photographs to be higher up the canyon wall (Figs. 1b and 2b). We therefore interpret this outcrop of pyroclastic material as representing part of the pyroclastic breccia emplaced within the evolving vent during its formation, rather than as part of the pyroclastic apron, though these two deposits may be related to one another (Valentine & Cole 2021).

Fig. 3 Schematics showing the structure of the Mule Creek vent in cross-section. Numbers in circles indicate figures that show the textures of the different features drawn here. **a** Vent structure towards the canyon rim as identified by Stasiuk et al. (1996). **b** Conduit structure as identified from the outcrop HMC09, see Fig. 1b for location. The outermost part of the vent consists of pyroclastic breccia, which is texturally very similar to the surrounding pyroclastic apron. Adjacent to the pyroclastic breccia is a unit of vitrophyre breccia, with glassy, often jigsaw-fit clasts that become more sheared and compacted towards the vent centre. The vitrophyre breccia grades inwards to become a more coherent vitrophyre unit. The vitrophyre grades into the rhyolite lava unit that forms the vent centre. The rhyolite lava unit is flow banded with flow bands that become more widely spaced towards the vent centre. Every unit of the conduit is cross-cut by tuffisite veins, with subvertical tuffisites in the rhyolite lava and vitrophyre units. In the vitrophyre breccia and pyroclastic breccia, tuffisites dip less steeply. Some tuffisites are laterally continuous, up to 13 m in length, while other tuffisites can only be followed for up to 50 cm



The structure of the pyroclastic breccia is complex, formed of multiple stratified subunits distinguished by their overall grain size and componentry. The outer subunits are exposed at the base of the outcrop where they form sub-horizontal layers that grade into one another (Fig. 6). Closer to the vent center, the pyroclastic breccia subunits

dip steeply towards the vent center before becoming subvertical, with a greater number of steep erosive surfaces. Many subunits contain slump features and steeply dipping extensional faults that offset subunit contacts by up to tens of centimeters (Fig. 7a). Faults are differentiated from slump or erosive features as more planar features,

Fig. 4 Logs of the maximum clast size and % lithics in the different pyroclastic breccia subunits in **a** Stasiuk et al. (1996), measured close to the canyon rim and **b** this study in outcrop HMC09. Componentry was completed at outcrop-scale (clasts > 2 cm across). Locations of both logs are marked on Fig. 2b. The trace of the log from outcrop HMC09 is drawn on Fig. 6b

confined to the pyroclastic breccia that offset sections of an identifiable subunit.

The different subunits of the pyroclastic breccia contain sub-angular clasts of the andesite host rock as well as rounded pumice clasts. There are varying clast sizes, with coarser subunits containing ≤ 30 cm lithic (non-juvenile) clasts and ≤ 80 cm pumice clasts, while finer grained deposits contain ≤ 2 cm clasts (Fig. 6). Sedimentary structures such as graded beds and coarser lenses of material are common in the finer grained subunits (Figs. 7a and b). A transect through the outcrop indicates highest lithic content towards its base (Fig. 4b). Some jigsaw-fit clasts are separated by thin ribbons of pyroclastic breccia (Fig. 7c). In some layers of pyroclastic breccia, the intergranular space between the larger clasts is filled with a matrix of densely welded fine-grained $< 5 \mu\text{m}$ particles (Fig. 7b).

The nature of the contacts between the various layers of pyroclastic material are highly variable, ranging from sharp, steeply inclined sub-vertical margins marked by a distinct, narrow glassy ‘rind,’ defined by its low vesicularity and absence of visible clasts at outcrop scale, to more complex and highly irregular morphologies with ‘feather-like’ interdigitating contacts. An example of a highly complex feather-like contact is shown in Fig. 8 where a laminated pyroclastic deposit composed of fine lapilli- and ash-sized grains is cross-cut by a relatively younger lithic breccia. Within a few centimeters of a sub-vertical contact running down the center of the photograph (Fig. 8a), the lamination is deflected upwards to become parallel to this glassy boundary (Fig. 8b).

Vitrophyre breccia and vitrophyre

The vitrophyre breccia and vitrophyre (Fig. 3) are lithologically very similar, forming subvertical dark-colored units with a glassy texture (Figs. 5b and c). These units are both non-vesicular. The vitrophyre breccia is a 0–3-m thick unit composed of mostly angular–subangular vitrophyre clasts (ranging from 1 to 10 cm across) and a few rare andesite clasts ~ 3 cm across (Fig. 5b; Stasiuk et al. 1996). The vitrophyre clasts often show a jigsaw-type fit, separated by red-colored welded clastic material, suggesting *in situ* fracturing of the material. However, Stasiuk et al. (1996) recorded some clast imbrication, suggesting at least some localized transport of clasts. Close to the contact with the vitrophyre (< 50 cm from contact) clasts become more elongate than those further from

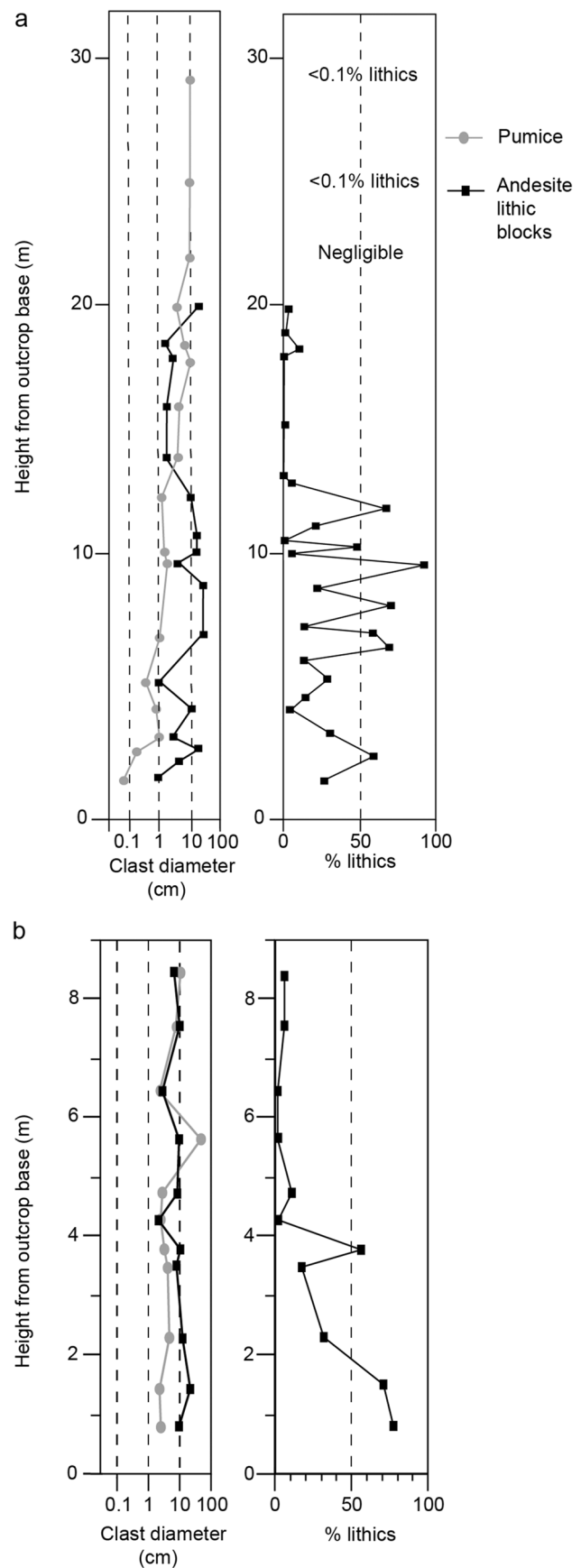
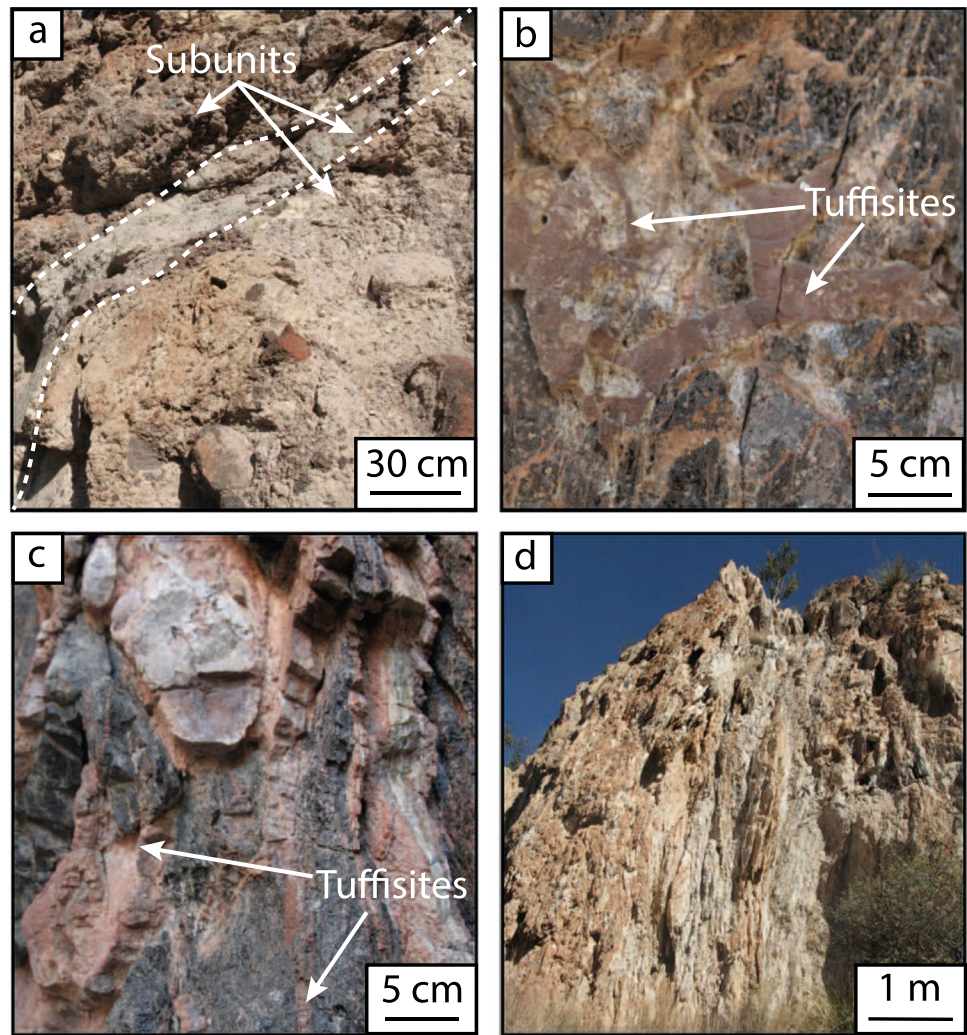


Fig. 5 Images of the main units within the Mule Creek vent. **a** Pyroclastic breccia consisting of multiple different subunits of varying grain size. **b** Vitrophyre breccia consisting of vitrophyre clasts (black/dark gray in color) heavily dissected by tuffisite veins (red-brown in color). **c** More coherent vitrophyre unit with vertical banding, with vitrophyre (black/dark gray in color) intersected by tuffisites (red-brown in color) and late-stage mineralization (white in color). **d** Central vent rhyolite lava showing well-developed platy fracturing



the contact, indicative of shear deformation parallel to the vent margins, and clasts are also more strongly welded together (Stasiuk et al. 1996).

The vitrophyre unit is typically ~1 m thick but locally reaches 7 m. Elsewhere within the vent, this vitrophyre unit can be absent (Stasiuk et al. 1996). Flow bands 1–100 μm thick in the vitrophyre are seen to be parallel to the vent margins in oriented samples but can be contorted and discordant where the contact is irregular (Fig. 5c; Stasiuk et al. 1996). The vitrophyre grades into the central rhyolite lava unit.

Flow-banded rhyolite lava

The innermost 25 m (measured from an approximate conduit center-line close to the canyon base) of the MCV is composed of grey to pink flow-banded rhyolite lava (Figs. 3 and 5d). The flow banding is more narrowly spaced (< 0.5 mm thick) towards the margins of the rhyolite lava compared with the unit centre (Fig. 3b). Towards the

center of the MCV the flow banding becomes relatively wider spaced and increasingly deformed by open to tight, steeply inclined isoclinal folds (Stasiuk et al. 1996). The flow bands consist of layers mostly defined by variations in the degree of vesicularity of the rhyolite lava, with some layers containing clearly visible, open subrounded vesicles, while other layers are less vesicular in appearance and display deformed coalesced vesicles (Stasiuk et al. 1996). Some flow bands are instead defined by alternating bands of aligned microlites and cryptocrystalline rhyolite. The coarsely flow banded rhyolite lava at the very center of the conduit is the most vesicular compared with the outer parts of this unit at outcrop scale. This unit shows well-developed sub-vertical platy fracturing (Fig. 5d). Small sub-millimeter spherulites in the center of the rhyolite lava increase in size and abundance towards the rhyolite lava margins, before decreasing once again where the rhyolite lava grades into the adjacent vitrophyre unit over a zone approximately 1 m thick (Stasiuk et al. 1996).

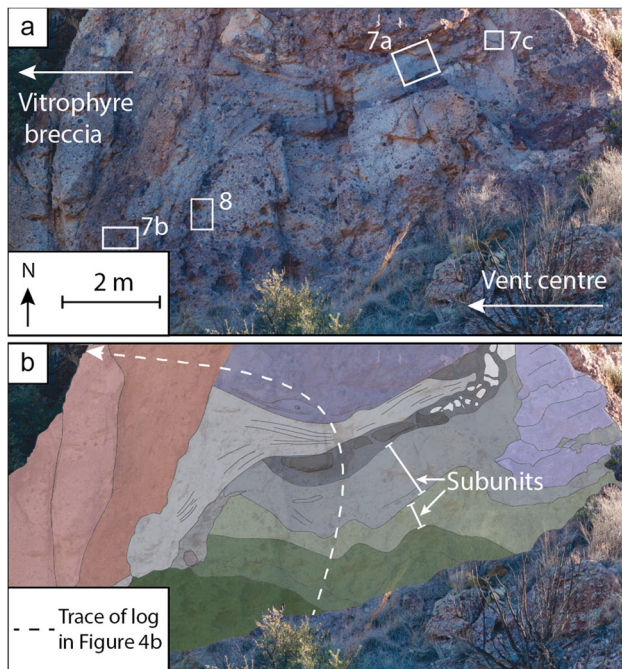


Fig. 6 Photograph (a) and interpretation (b) of outcrop HMC09. The pyroclastic breccia is composed of multiple cross-cutting subunits, suggesting repeated erosion and deposition of material. The white dashed line shows the trace of the lithostratigraphic log in Fig. 4b. The colored subunits in (b) highlight rock subunits of different characteristics, such as different proportions of lithics

Pyroclast-filled fractures

Pyroclast-filled fractures have been recognized in each different unit of the MCV (Fig. 3) and typically form cross-cutting veins that record fluid transport and injection into the host rock. The size of these veins varies considerably from laterally extensive features which are > 30 m in length to much shorter veins that can only be followed for ~2 cm. The morphology of the pyroclast-filled veins varies depending on their host lithology. Consequently, we have divided the veins into the following categories—those hosted in (1) country rock, (2) pyroclastic breccia, (3) vitrophyre or vitrophyre breccia, (4) cross-cutting multiple units, and (5) flow-banded rhyolite lava. The characteristics of the pyroclast-filled veins within each host rock are summarized in Table 1. Many of these observations are similar to those found closer to the top of the canyon by Stasiuk et al. (1996).

Pyroclast-filled veins hosted in the country rock

The mostly sub-horizontal pyroclast-filled veins (~2 cm in width) within the country rock extend into the surrounding Bearwallow Mountain andesite or pyroclastic apron (Fig. 3; Stasiuk et al. 1996). The veins divide into multiple narrower veins (< 1 cm in width) at their tips to produce a branching

network (Figs. 3 and 9a and b; Stasiuk et al. 1996). The veins are filled with a matrix of red, oxidized, ash-sized particles with fragments of quartz and feldspar phenocrysts and larger (< 1 cm across), subangular clasts of rhyolite lava and andesite (Stasiuk et al. 1996). Laminations and cross-laminations are common in the finer ash-sized particles found at the fracture margins.

Pyroclast-filled veins hosted in the pyroclastic breccia

Pyroclast-filled veins in the pyroclastic breccia are typically ~5 cm in width with diffuse margins, giving veins a wispy appearance (Figs. 9c and d). The fill is entirely composed of ash-sized particles that are typically welded (<5 μm across; Figs. 10a and 10b). This material has a similar appearance to the matrix of the pyroclastic breccia and the material forming tuffisites in the country rock, suggesting a similar composition. The finest material is at the fracture margins where it forms sub-horizontal to irregular, finely laminated features that infill originally open pore spaces and/or voids within the host breccia. Clasts of host material also sometimes protrude across vein margins (Fig. 11a) and clasts from the host breccia that are substantially larger than those of the surrounding vein material can also be found at vein centers (Fig. 11a). This is in contrast to tuffisites seen elsewhere that occur within fractures. Within the pyroclastic breccia, the clast-filled veins were observed forming isolated areas of fine-grained material that are not apparently connected to the margin of a pyroclastic breccia subunit, though could be connected in 3D.

The pyroclastic breccia-hosted veins typically contain complex internal structures, including laminations, climbing ripples, and internal self-injections (Fig. 11b). The host pyroclastic breccia adjacent to the veins has experienced soft-sediment deformation, with localized vein-adjacent fluidization producing complex structures including disharmonic folds, cuspsate to irregular boundaries between the laminated vein and breccia (Fig. 11a), and the disruption of the matrix to the breccia to form ‘ball-like’ structures enclosed within the vein (Figs. 11b and c). Soft-sediment deformation of the host pyroclastic breccia was also observed and associated with the fragmentation of these fine-grained pyroclast-filled veins themselves, which are broken up into jigsaw-fit clasts of densely welded material.

Pyroclast-filled veins hosted in the vitrophyre and vitrophyre breccia

Pyroclast-filled veins within the vitrophyre are mostly oriented sub-vertically, parallel to the banding within the vitrophyre (Fig. 5c). Most of the veins are too narrow (< 1 mm in width) to contain visible internal structure and are filled with brown-colored altered devitrified material, with fuzzy

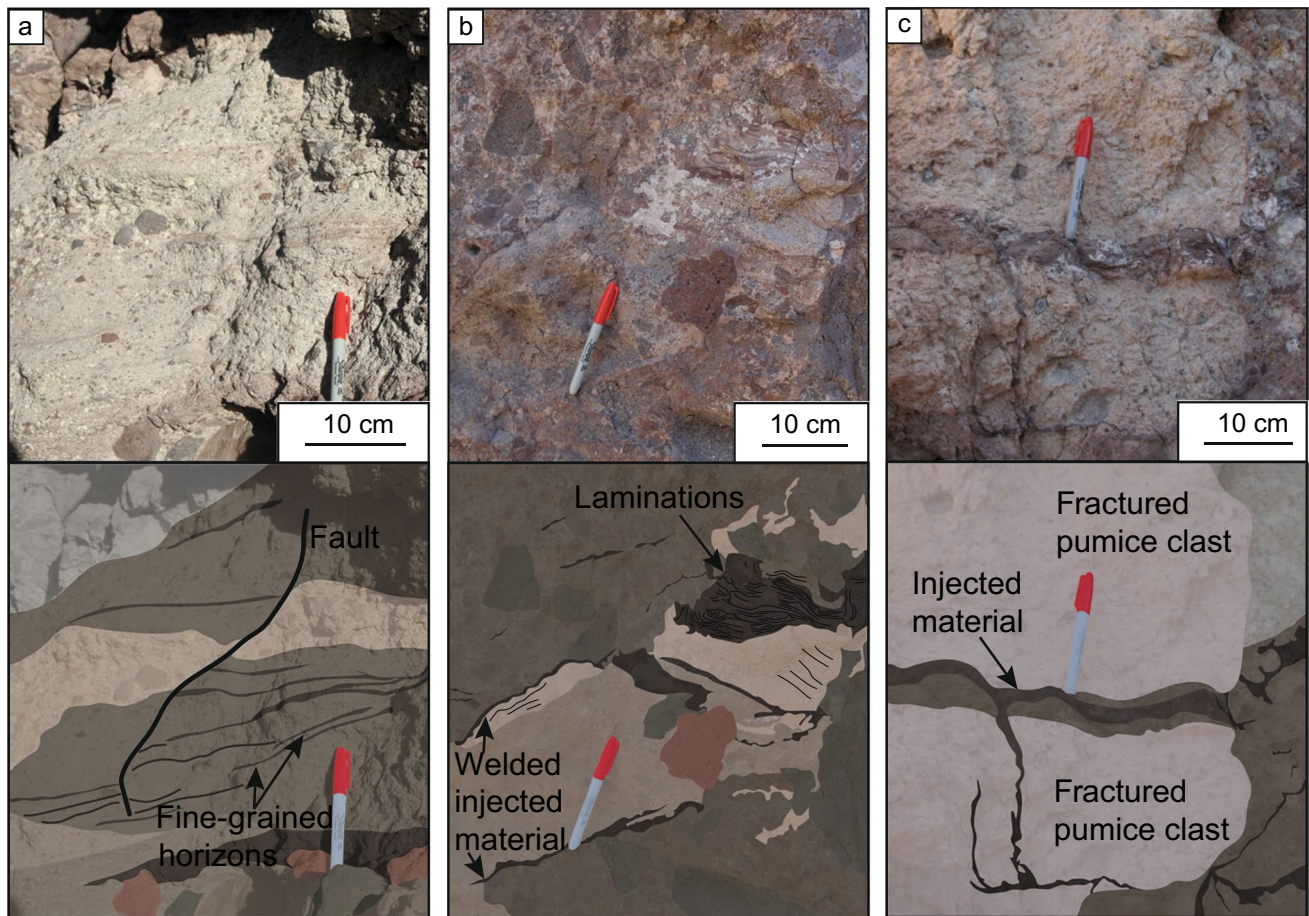


Fig. 7 Photographs of structural features in the pyroclastic breccia (top) and interpretations (bottom). Different colors are used to distinguish between subunits of different appearances. **a** A finer grained subunit within the pyroclastic breccia showing laminations, cross-

lamination, and coarser lenses of lapilli-sized material, offset by a small fault. **b** Finer grained horizons of ash-sized particles cross-cutting the surrounding pyroclastic breccia. **c** A fractured pumice clast ~50 cm across injected with clastic material

local alteration also affecting the fracture walls along the fracture length.

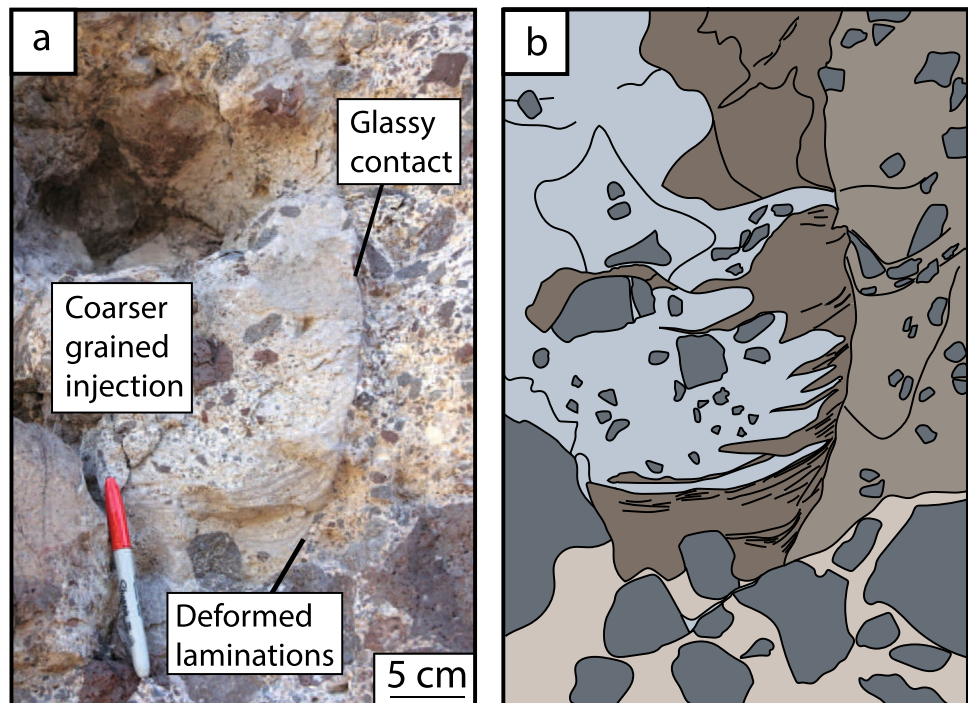
Many pyroclast-filled veins within the vitrophyre-breccia have the same appearance as those in the vitrophyre. However, some fractures within the vitrophyre breccia are larger, up to 1 cm in width, and contain either discontinuous laminae or irregular patches or clasts of clastic material resulting in complex internal structures (Figs. 5b and 11d). The fracture margins are often lined with vitrophyre fragments up to 20 μm across (Fig. 10c) that are welded—locally to such an extent that the individual clasts are no longer visible (Fig. 10d). Horizons of ash-sized particles, angular vitrophyre clasts, and crystal fragments weave between those vitrophyre blocks. The clast-filled veins can also contain irregularly shaped blobs of melt with microlites that can be aligned in sheared clasts (Fig. 10d). The microlite texture of each of the melt blobs is qualitatively similar and the melt blobs are much more microlite-rich than the surrounding vitrophyre. Narrower veins within the vitrophyre breccia have structures

that are less complex, but often still show cross-cutting relationships. The erosive contacts between the different injected domains are sharp, with no indication of soft-sediment deformation. These veins do not show other internal structures such as cross-bedding or lamination (Fig. 11d).

Cross-conduit pyroclast-filled veins

Pyroclast-filled veins are not restricted to spanning the width of one vent unit, and Stasiuk et al. (1996) reported laterally extensive veins originating in the vitrophyre breccia and continuing outwards through the pyroclastic breccia and into the surrounding andesite country rock. In this study, one laterally extensive vein with a length > 30 m was traced through the pyroclastic breccia and into the country rock (HMC07, Figs. 2a and 3b). These veins have a similar appearance to the matrix of the pyroclastic breccia and the pyroclastic breccia-hosted tuffsites, suggesting a similar composition.

Fig. 8 Photograph (a) and interpretations (b) of the pyroclastic breccia surrounding a steeply dipping glassy contact within the pyroclastic breccia that separates finer laminated material from a much coarser-grained subunit. Laminations in the finer material onlap onto the glassy contact



Pyroclast-filled veins hosted in flow-banded rhyolite lava

The pyroclast-filled veins within the rhyolite lava are typically ~2 cm wide and tens of centimeters long and steeply dipping, aligned parallel to flow banding within the host rock (Fig. 9e; Stasiuk et al. 1996). The internal structure of these veins is complex, with sharp well-defined erosive to gradational contacts separating clastic domains with different grain sizes. Soft-sediment deformation is clearly seen, with curved walls to injections and deformed laminations. The pyroclast-filled veins can form an angular network filled with welded material.

Interpretations

The units of the MCV are interpreted to have all been emplaced during a waning explosive eruption, forming in order from the pyroclastic breccia at its outer margins deposited first, then cross-cut by the accretion of the vitrophyre breccia and vitrophyre, before finally the emplacement of the rhyolite lava within the centre of the evolving vent (Fig. 12 and animation (Online resource 2)). Repeated fracturing and the injection of material into the vent units would have been facilitated by pulsations within this overall waning phase.

Formation of the pyroclastic breccia

The different subunits of the pyroclastic breccia are often separated by erosive surfaces, suggesting repeated cycles of

erosion and deposition. The extensional faults seen within the pyroclastic breccia (Fig. 7a) reflect material collapsing back into the vent at the end of a phase of deposition. Sub-horizontal subunits away from the vent center are interpreted to have formed first, cross-cut by later subunits deposited closer to the vent center (Fig. 12 and animation (Online Resource 2)). Welding of the pyroclastic breccia allowed it to transition from a loose pile of fragmented rock and pyroclasts that would have been frequently overturned to a more coherent rock. Later sub-vertical pyroclastic breccia would have been injected through this more coherent material, allowing steeper and better-defined erosive contacts to form. Fractured jigsaw-fit clasts separated by ribbons of clastic material (Fig. 7c) record a smaller-scale version of this process, with sudden pressure pulses breaking clasts during deposition.

The pyroclastic breccia contains a substantial volumetric proportion of lithic clasts, suggesting that the breccia was emplaced during an early stage of vent formation when explosive processes were quarrying, transporting and depositing clasts of the surrounding country rock (Fig. 4; Stasiuk et al. 1996). The erosive contacts suggest that significant erosion was still occurring, interspersed with periods of deposition. The lower lithic clast proportion (< 10 vol.%) in the later sub-vertical pyroclastic breccia subunits could indicate that earlier breccia subunits acted as a barrier preventing further quarrying of the country rock (Fig. 4). Through time, subunits became less lithic-rich as the conduit began to stabilize in both size and shape, reducing the overturning of the pyroclastic

Table 1 The characteristics of the pyroclast-filled veins found within the different units of the Mule Creek vent

Fracture morphology and margins	Country rock		Pyroclastic breccia	Vitrophyre breccia	Vitrophyre	Cross-cutting multiple host rock units	Rhyolite lava
	Bearwallow Mountain andesite	Pyroclastic apron					
Fracture morphology and margins	Irregularly shaped fracture margins		Diffuse margins giving a wispy appearance	Sharp-edged fracture networks	Sub-vertical sharp-edged fractures parallel to banding in vitrophyre	Diffuse margins coated with fine ash-sized particles	Wavy fractures with poorly defined margins parallel to flow banding
Fracture length	Fractures typically laterally continuous for a few meters Extend up to 10 m into country rock before branching into networks of veins < 1 cm wide		Generally tens of cm in length but up to 1.3 m long	Wider main fractures show a greater degree of fracturing of their vitrophyre walls	Fractures laterally continuous for < 1 m Small perpendicular offshoot fractures extend a few cm from the main fracture	Fractures up to 30 m in length Extend from the margin of the vitrophyre breccia, through the vitrophyre and into the country rock	Fractures ~10 cm in length
Fracture width	Fractures up to 10 cm in width	Fractures up to 20 cm in width	Fractures typically < 5 cm in width	Fractures up to ~1 cm in width	Fractures up to ~5 mm in width	Fractures up to ~20 cm in width	Fractures typically ~2 cm wide
Fracture fill	Well sorted homogeneous lapilli-sized grains	Welded ash-sized particles < 5 μm across	Welded ash-sized particles < 5 μm across	Ash-sized particles, angular vitrophyre clasts, and crystal fragments	Brown-colored altered devitrified material at fracture center	Welded ash-sized particles < 5 μm across to lapilli-sized grains	Multiple domains of well sintered ash-sized particles
	Subangular rhyolite lava clasts < 5 mm across and quartz and feldspar phenocrysts		Particles fill pore spaces between large clasts in the breccia	Fracture margins lined with welded vitrophyre clasts up to 20 μm across	Fuzzy alteration affects the fracture walls along the length of the fracture	Large clasts in the fracture centre sourced from the surrounding host rock	Few quartz and feldspar phenocrysts < 0.5 mm across
	Andesite clasts < 1 cm across close to vein margins	Rare andesite clasts	Large clasts sourced from the breccia protrude across vein margins	Horizons of fine grained material weave through welded blocks of vitrophyre clasts			
Internal structures	Laminations and cross-lamination common		Laminations and climbing ripples	No laminations or cross-lamination	Most veins too narrow to contain visible internal structure	Lamination, cross-lamination and graded bedding	Laminations and graded bedding
	Jigsaw-fit andesite clasts at vein margins	More complex internal structure than andesite-hosted veins	Internal self-injections	Wider fractures contain multiple domains of material separated by sharp erosive contacts	Continuous pale band of glassy material at center of largest fractures	Multiple domains separated by sharp well-defined erosive to graded contacts	Multiple domains separated by sharp erosive contacts
			Soft sediment deformation of vein adjacent material	Narrower fractures have a more simple internal structure with fewer domains		Soft sediment deformation of vein adjacent material when hosted by pyroclastic breccia or pyroclastic apron	Soft sediment deformation to produce deformed laminations

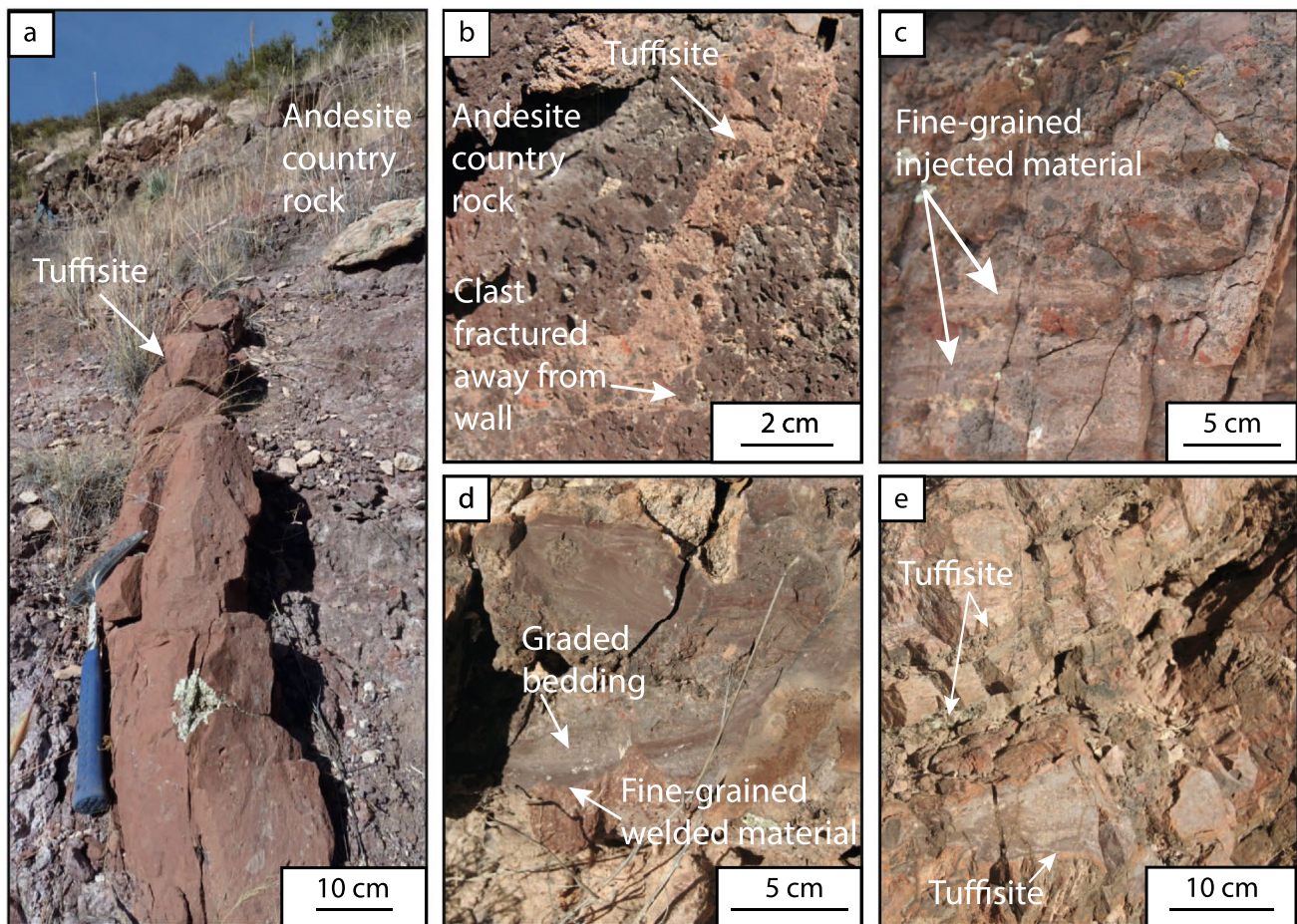


Fig. 9 Photographs of tuffisites in different units of the Mule Creek vent. **a** Tuffisite (red, in center of image) in the andesite country rock surrounding the vent. **b** Tuffisite in the andesite country rock containing clasts derived from the tuffisite walls. **c** Sub-horizontal fine-

grained tuffisites cross-cut pyroclastic breccia. **d** Tuffisite hosted in pyroclastic breccia displays complex laminations and graded bedding. **e** Tuffisites within the vent rhyolite form a network of veins with a glassy appearance

breccia already deposited and breaking less material from the conduit walls (Valentine & Cole, 2021).

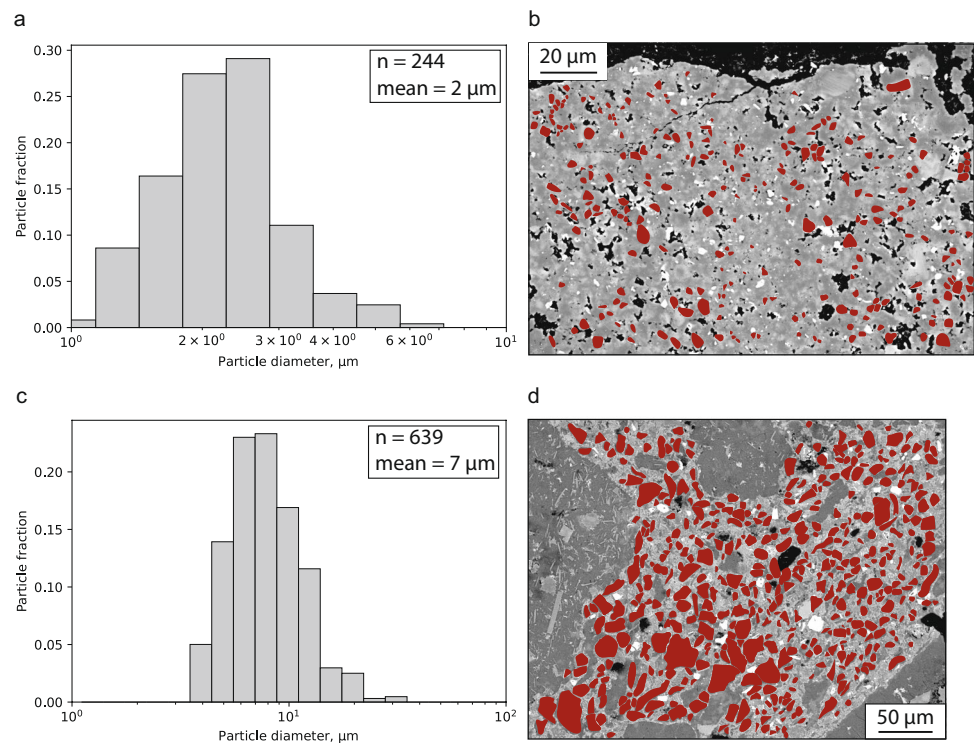
The steep glassy contact (Fig. 8) is an example of one of the erosive margins between different breccia subunits. Its glassy margin formed via accretion of ash-sized particles to the sub-vertical surface, where they could weld to form dense glass, through the same processes thought to form obsidian or vitrophyre at conduit margins (Gardner et al. 2017). The formation of the glassy margin suggests that this position in the vent was sufficiently hot for welding to occur, and if deposited rapidly enough, this may have helped to strengthen the margin, allowing it to exist at such a steep angle.

Formation of the vitrophyre breccia and vitrophyre

The similarities between the vitrophyre breccia and vitrophyre units, both dark units with a glassy appearance and

low vesicularity, suggest that these units are formed of the same material. These units are therefore interpreted to have formed through the same process, with the vitrophyre breccia a brecciated derivative of the vitrophyre. The vitrophyre is formed by the hydration of obsidian due to post-emplacment alteration. Obsidian can form by the accretion of pyroclasts at the conduit margins (Online Resource 3; c.f. Gardner et al., 2017), and if continued this process could also produce a thick unit coating the conduit walls (Wadsworth et al. 2020). This is the same process that we suggest formed the thin, localized glassy contact within the pyroclastic breccia (Fig. 8; see “Formation of the pyroclastic breccia”), but here occurring on a far larger scale in terms of both the thickness and vertical continuity of the dense glassy layer formed. The lack of lithics in the vitrophyre breccia and vitrophyre suggest that quarrying of the country rock had decreased by the time these units were emplaced, perhaps

Fig. 10 Grain size distributions of particles seen in SEM images. The particles measured are colored in red in the SEM image, and n is the number of particles measured. **a, b** Particles forming a diffuse tuffisite within the pore space of the pyroclastic breccia. Image location is given in Fig. 11a. **c, d** Particles forming a tuffisite within the vitrophyre breccia. The location of the SEM image is given in Fig. 11d. The original untraced images can be found in Online Resource 1



due to the source of lithics becoming cut off as the margins of the conduit were no longer country rock, or because explosivity waned.

There are two potential mechanisms by which the vitrophyre could brecciate to form the vitrophyre breccia: either the latter formed through *in situ* fracture of a coherent vitrophyre, supported by the pseudo-jigsaw-fit appearance of many clasts and the presence of tuffisites, or clasts were eroded and transported from greater depth, before being deposited to form the vitrophyre breccia (Gardner et al. 2017; Wadsworth et al. 2020). Compaction and shearing later altered the shape of these clasts towards the vitrophyre breccia–vitrophyre contact (Fig. 3), causing them to become more elongate, masking the evidence for these processes across much of the unit.

The persistence of lithics suggests some clasts within the vitrophyre breccia were sourced from elsewhere, perhaps sourced from a greater depth and transported up the conduit to their place of deposition (Stasiuk et al. 1996; Saubin et al. 2016). Imbricated clasts must have been transported at least a few metres before being deposited. Most clasts however have a jigsaw-fit appearance, suggesting that while some clasts may have been transported from elsewhere, the local clast production by *in situ* fracturing was more prevalent (Online Resource 3). Shear traction on the assembling vitrophyre walls due to the bypassing high velocity gas and pyroclasts could produce a sufficiently high shear stress, relative to the elastic shear modulus, to brecciate the vent margin (Wadsworth et al. 2018). If the brecciation of the vitrophyre

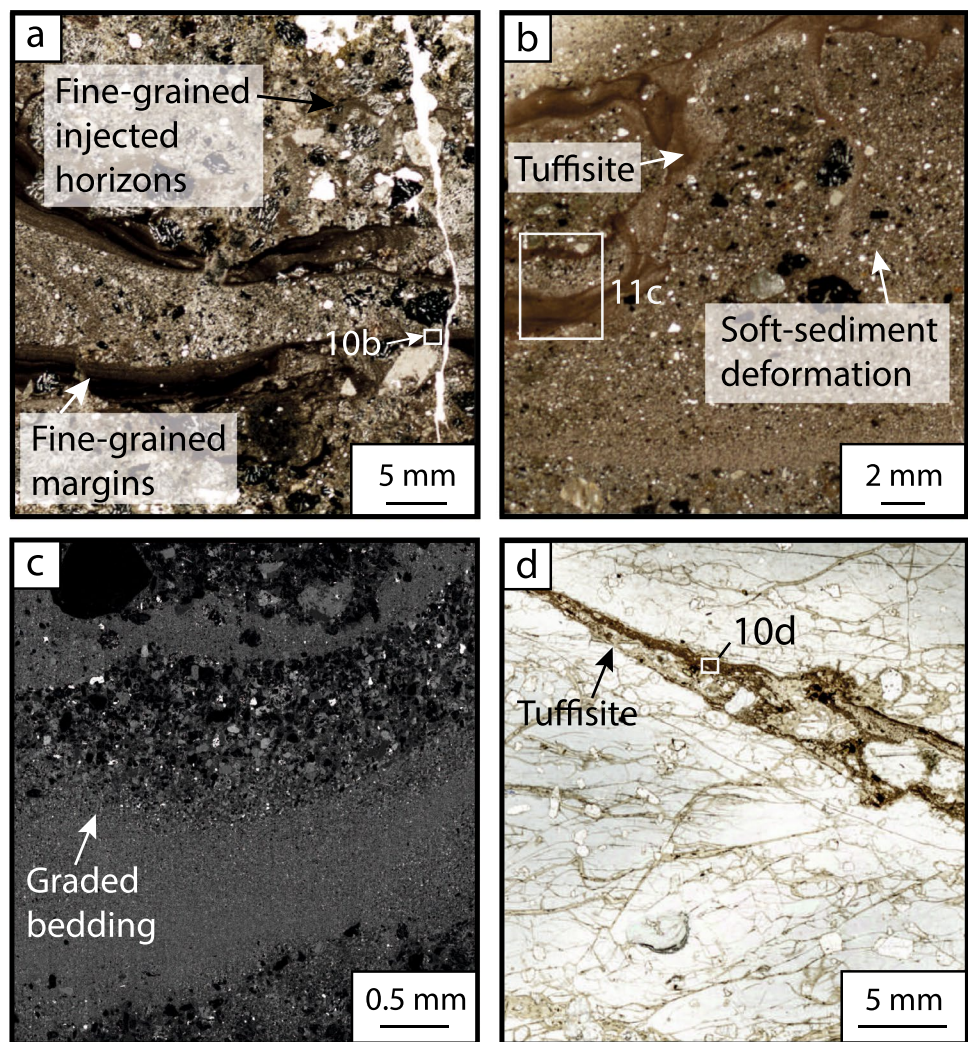
walls is indicative of high velocity bypassing flow, then the transition to non-brecciated vitrophyre could represent eruption waning and a further reduction in explosivity, as dense conduit-plugging material experienced a lessening degree of damage by pulses of pressurized magmatic fluids.

Formation of tuffisites

The pyroclast-filled veins found cross-cutting the different vent units are interpreted as tuffisites, with all veins except those in the pyroclastic breccia occurring within fractures. We interpret the fracture-hosted tuffisites as hydrofractures driven by pressurized magmatic fluids (gas–pyroclast mixtures) above the fragmentation level in the eruption-feeding conduit (Wadsworth et al. 2020; Unwin et al. 2021). Most of the tuffisites seen within the MCV have complex internal structures that must reflect either variations in the fluid velocity along the fracture or changes in fracture width, or both. Variations in fluid velocity can be driven either externally, by gas pressure fluctuations within the volcanic conduit, or internally by local variations in the fracture width, created by pre-existing narrower fracture sections or by clogging the fracture with deposited material (Perkins & Kern 1961; Cosgrove 2001; Phillips et al. 2013; Unwin et al., 2021).

Within the MCV we identify four different phases of tuffisite formation: (1) the formation of tuffisites within the country rock, associated with the opening of the conduit pathway (Figs. 9a and b), (2) diffuse tuffisites within the pore space of the pyroclastic breccia (Figs. 9c and d), (3)

Fig. 11 Photomicrographs and SEM images tuffisites within the pyroclastic breccia and vitrophyre breccia. White labelled boxes indicate the position of SEM images within the larger scale image. **a** Photomicrograph of a tuffisite within the pyroclastic breccia, with finely laminated margins. The injected material grades into coarser particles towards the tuffisite center. **b** Photomicrograph of tuffisite in the pyroclastic breccia, with irregular margins, formed of fine-grained laminated material, and a coarser center. **c** Backscattered electron image of fine-grained injection within the pyroclastic breccia. Small ash-sized particles fill the pore space of the host breccia. **d** Sharp-edged tuffisite within the vitrophyre breccia containing different phases of injected material separated by erosive surfaces



tuffisites hosted within the vitrophyre and vitrophyre breccia (Figs. 5b, 5d, and 11d), and (4) tuffisites within the central rhyolite lava (Fig. 9e).

Tuffisites in the country rock

Tuffisite veins within the andesite country rock contain clasts of the host rock at their margins that have been fractured away from the vein wall (Figs. 9a and b). This fracturing process records the propagation and widening of the fracture network, with country rock tuffisites recording the first stages of vent evolution (Cloos 1941). These tuffisites record some of the first fractures that were opened as part of the fracture network that developed into the MCV. Parts of the fracture network that have been abandoned and not destroyed during the quarrying of the vent can be filled with pyroclastic material and preserved as tuffisites within the country rock (Fig. 12 animation (Online Resource 2)).

The diffuse margins of tuffisites hosted by the pyroclastic apron reflect the difficulties of opening and propagating a pathway through the highly permeable host rock. Instead, gas escape exploited, and potentially widened, pre-existing open voids and intergranular pore spaces within the breccia, which progressively filled with laminated/stratified ash. Deposition of these tuffisite cavity fills would have led to a locally significant reduction in the permeability of the pyroclastic apron, acting to seal areas of the evolving vent margins.

'Early' tuffisites in the pyroclastic breccia

The tuffisites within the pyroclastic breccia are not fracture hosted, but instead comprise fine-grained materials likely swept through the pore space of the surrounding pyroclastic breccia and driven by lateral pressure gradients within the volcanic conduit (Fig. 11a and b). Particles carried into the pore space would likely be deposited either where the fluid pressure decreased as it entered a larger void, or where the

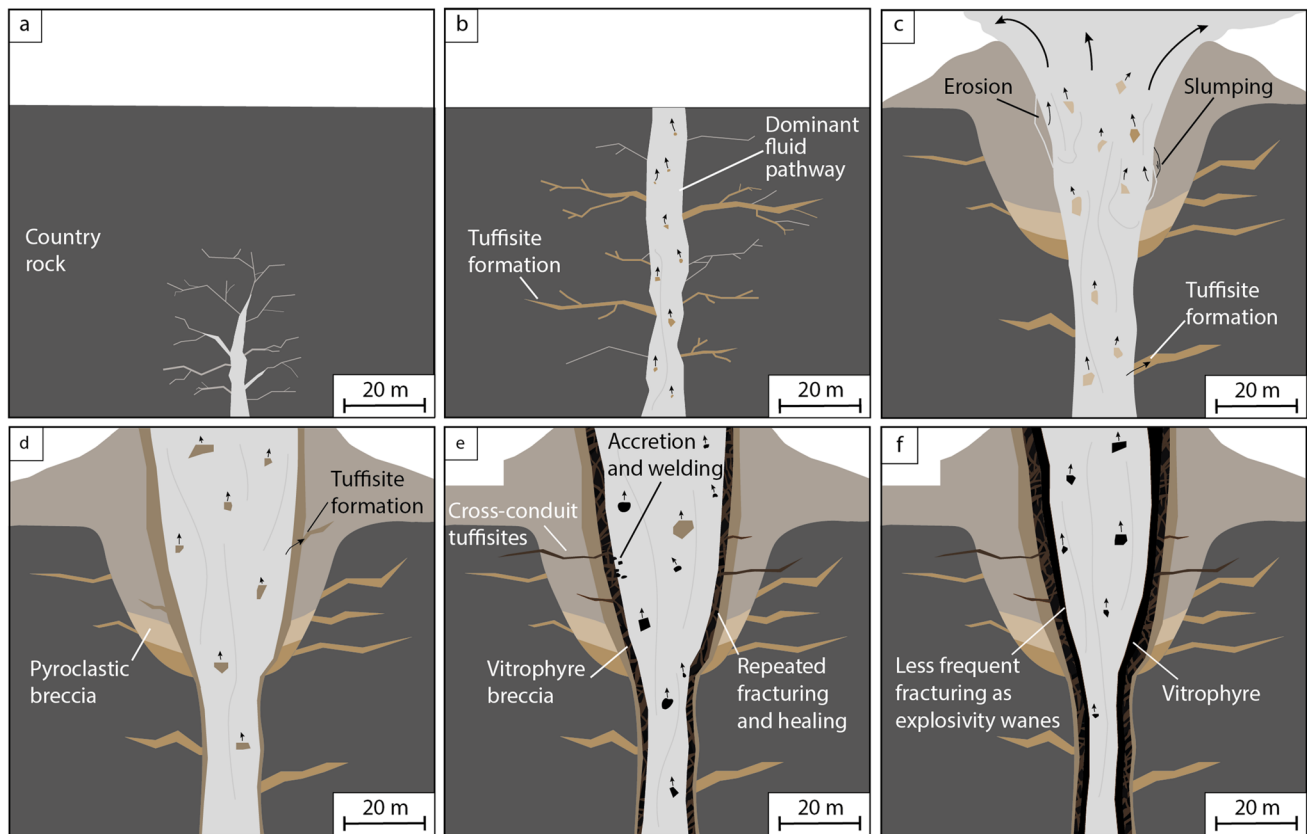


Fig. 12 Model for the formation of the Mule Creek vent. See animated version of this figure (Online Resource 2). **a** Fractures are opened by a high-pressure gas–pyroclast mixture. If preserved, material deposited within these fractures forms tuffsites within the country rock (e.g., Fig. 9a). **b** Continued fracturing forms a network of fractures that can grow in size (thickness and length) due to the quarrying of pyroclastic material. **c** Propagation and widening of fractures allows for the formation of a proto-conduit. **d** Repeated deposition and erosion as fluid pressure within the developing conduit fluctuates allows for the emplacement of multiple subunits of pyroclastic

fluid flux was lowest. These tuffsites leave behind a record of this process in the areas of lower permeability or where fluid flow pathways become blocked. Unlike the tuffsites found in other vent units, these tuffsites are not formed by hydrofracturing, instead representing outgassing through dilation of existing permeable pathways that did not require fracturing to further increase permeability.

The soft sediment deformation surrounding these features reflects the passage of pressurized gas through the pore spaces of the unlithified breccia, which reduced the effective confining pressure, lowered its cohesive strength, and allowed for shifting and slumping. More extensive tuffsites (< 13 m in length) may represent areas where the fluid flow within the pyroclastic breccia was more constrained to a single pathway, allowing for more focused deposition of material into a single vein. These more laterally extensive tuffsite veins are consistent with the infilling of the

breccia. Pyroclastic breccia-hosted tuffsites can form (e.g., Fig. 9b–d). **e** Once the conduit reaches a great enough temperature, welding of ash-sized particles at the conduit margins produces the vitrophyre. Repeated fracturing and healing forms the vitrophyre breccia with jigsaw-fit clasts and vitrophyre breccia-hosted tuffsites. Cross-conduit tuffsites that intersect multiple vent units form. **f** Once the explosivity drops sufficiently, the accreting vitrophyre will not be as greatly fractured, producing a more intact vitrophyre unit. Fracturing of the vitrophyre by high-pressure gas–ash mixtures produces tuffsites hosted within the vitrophyre

pre-existing intergranular pore spaces and cavities, not only lowering the permeability of the breccia but also reducing the friability of these pyroclastic deposits, facilitating subsequent fracture development.

Tuffsites in the vitrophyre and vitrophyre breccia

The morphology of the tuffsites within the vitrophyre and vitrophyre breccia reflects the greater cohesion and lower permeability of the vitrophyre compared to the pyroclastic breccia. The wide variety of tuffsite orientations seen in the vitrophyre breccia (Fig. 5b) suggest that tuffsite formation is not necessarily controlled by pre-existing fabrics, although the branches at the margins of the tuffsite in Fig. 11d do exploit pre-existing fractures in the surrounding vitrophyre breccia. The more poorly developed fabric of the outermost parts of the assembling vitrophyre breccia would act as less

of a control on the morphology of intersecting tuffisites than the stronger fabric seen within the vitrophyre. The tuffisites within the vitrophyre and vitrophyre breccia were emplaced after the development of the fabric, once the vitrophyre had cooled sufficiently to have fractured by shearing, producing pathways that tuffisites could easily exploit.

The tuffisites in the vitrophyre breccia are interpreted as fracturing and injecting material into the stationary conduit wall, leading us to consider them to be external tuffisites, rather than internal tuffisites formed by *in situ* shear failure of highly viscous magma (c.f. Stasiuk et al., 1996, Tuffen et al., 2003). The interpretation of the vitrophyre forming by accretion at the conduit margins suggests that these tuffisites formed instead as external tuffisites by tensile failure, with some clasts broken from the fracture walls as the fracture opened, and other clasts injected.

Some obsidian-hosted tuffisites described elsewhere are angular particle-filled fractures that have developed tractional bedforms (Tuffen et al. 2003; Tuffen & Dingwell 2005), and display very similar morphologies and internal structures to the Mule Creek vitrophyre breccia and vitrophyre-hosted tuffisites. These were originally documented at Torfajökull, Iceland, and interpreted as internal tuffisites. In that interpretation, the clastic fracture fill was thought to be locally derived clasts from fracture walls (Tuffen et al. 2003). However, the observations made herein suggest that these similar features may actually have been external tuffisites with clastic fill sourced from an erupting and bypassing dispersion travelling up a volcanic conduit prior to conduit sealing by continued welding. This reinterpretation would provide a source for the trace metal concentrations in the Torfajökull veins, which Berlo et al. (2013) attributed to a genesis that was ‘deep’ relative to the tuffisite position. Similarly, the observations made here suggest that the pyroclasts filling tuffisites found in vitrophyre-like bombs, such as the bomb documented by Saubin et al. (2016), may be sourced from magmatic fragmentation, contrary to models that suggest that the fill is formed by disaggregation of a foamy magma directly beneath the vitrophyre. Taken together, these comparisons between the MCV vitrophyre-hosted tuffisites and similar tuffisites found elsewhere lend support to models that envisage the shallow conduit as progressively plugging by sintering of the products of deeper fragmentation (Wadsworth et al. 2020, 2022; Farquharson et al. 2022). We propose that tuffisites can be considered to be predominantly *external* rather than internal, as a large proportion of their fill is distally derived, and carried through tensile fracture networks within largely passive, conduit-lining dense magma. The particle source is the deeper gas-ash-pyroclast mixture feeding the ongoing eruption, consistent with models for combined explosive–effusive eruption behavior (Wadsworth et al. 2020), and failure is driven by gas overpressure (Unwin et al. 2021). This model provides a distinct fluid and particle source able to fluidize and transport

particles within the tuffisite and emphasizes the passive role of the dense conduit lining over the timescale of overpressure-driven brittle failure events, even if it remained capable of some viscous deformation.

Tuffisites hosted in flow-banded rhyolite lava

Tuffisites within the central flow-banded rhyolite lava (*internal tuffisites*) have previously been proposed to form by the same mechanisms as those in vitrophyre or obsidian and are often considered to form when stresses within magma meet or exceed the magma shear strength, opening networks of magma-hosted fractures (Tuffen et al., 2003; Tuffen & Dingwell 2005; Kendrick et al. 2016; Paisley et al. 2019). The tuffisites within the rhyolite lava of the MCV are steeply dipping, reflecting either failure parallel to the plane of maximum shear stress, rotation of veins by subsequent viscous flow and shear (Tuffen et al. 2003; Gonnermann & Manga, 2003), or exploitation of weaker pore-rich bands associated with devitrification (Schipper et al. 2015).

The clasts in internal tuffisites have previously been thought to derive entirely locally from fracture walls (Tuffen et al., 2003; Tuffen & Dingwell 2005), or from a foamy magma immediately beneath, and in contact with, a dense magma plug (Saubin et al. 2016). Neither of these models is consistent with the observed lithic content of internal tuffisites (Heap et al. 2019). Flow banding in the central rhyolite lava at the MCV and the granulation at the margins of lava plugs elsewhere demonstrate that the lava plug is pushed upwards and out of the vent (Pallister et al. 2013; Gaunt et al. 2014). Tuffisites in the vent center will therefore also likely be deformed (Tuffen et al. 2003), changing their planar geometry, and obscuring their relationship with particle sources. For this reason, as suggested in “Formation of tuffisites,” we propose that it is consistent with our genetic model to assume that what appear to be internal tuffisites may be consistent with flow-deformed external tuffisites. These fractures within conduit-blocking magma, assembled by the welding of pyroclastic material, provided pathways for pyroclastic material produced by continued fragmentation at depth to reach the surface during hybrid explosive–effusive activity (Wadsworth et al. 2020, 2022; Schipper et al. 2021).

A model for the formation of the Mule Creek vent

It follows from our interpretation that the material at the conduit center is relatively younger than the material forming the conduit margins, and as such, each conduit unit records a different period of conduit evolution. Tuffisites are found within every unit of the MCV, formed at different stages of conduit evolution

and at a variety of scales, with very few cross-cutting the entire conduit width. This indicates that there was a continuous but pulsating supply of pyroclastic material to feed tuffisite formation during vent evolution.

Conduit opening and the erosive formation of the vent structure

The propagation of fractures by pressurized gas-pyroclast mixtures through the overlying andesite created pathways for fluid flow (Fig. 12a and animation – Online Resource 2). A branched network of fractures formed, exploiting the weakest pathways for fracture opening (e.g., bed/unit contacts, joints, and faults). Where this propagating fracture network separated blocks from the surrounding country rock, these could become entrained into the ascending fluid, providing a source of the lithic clasts. Variations in fluid velocity, driven by fluctuating fluid pressure, would have caused pyroclastic material and country rock fragments to be deposited within the opening fractures (Fig. 12b). Through time, the network of fractures was refined into a major pathway with a simpler shape, forming an evolving conduit. Some abandoned pyroclast-filled fractures may be preserved, forming tuffisites that cut through the country rock adjacent to the major pathway.

The onset of vent-filling emplacement of the pyroclastic breccia

Once a vent is opened the initial activity is likely to be purely erosive and would therefore not be recorded in any vent-filling units. The pyroclastic breccia unit was the first within-vent unit emplaced during conduit formation. A relatively high proportion of country rock fragments records the quarrying and filling of space with pyroclastic material and fragments of country rock, together with pyroclastic material (Fig. 4). The first subunits deposited are subhorizontal, as the quarried-out area is filled with pyroclastic material, but repeated erosion and deposition produces later subunits that dip more steeply towards the conduit center (Fig. 12c). The permeable pyroclastic breccia filling the evolving conduit would allow for lateral outgassing from the conduit, with erosion, deposition and slumping causing the fluid pathway to migrate and seal through time. Ash-sized particles transported into the pore space of the surrounding pyroclastic breccia by outgassing can be deposited to form what we term ‘diffuse tuffisites’ (Fig. 12d).

At Cordón Caulle, Chile in 2011 and Chaitén, Chile in 2008, the initial purely explosive phase of activity lasted about ten days (Lara 2009; SERNAGEOMIN-OVDAS 2011). If the Mule Creek eruption had a similar timescale, the vent-filling breccia would be deposited over a similar period as the purely explosive phase waned and conduit occlusion prevailed, before the dense lava was produced and erupted.

Vent wall steepening and localization: a transition from unwelded pyroclastic breccia to welded vitrophyre breccia

The sustained input of fragmented material from depth would supply material to become trapped within the conduit. The continued deposition of hot material within the conduit and the increasing volume of the accreted deposits would have inhibited cooling of the conduit fill, enabling ever-greater welding of the surrounding pyroclastic breccia subunits (Kolzenburg et al. 2019).

Welding increased the cohesion of the pyroclastic breccia, stabilizing the conduit walls and preventing the overturning of the deposited material. The increased stability would also allow tuffisites hosted within the pyroclastic breccia to become larger and more extensive. As the permeability of the pyroclastic breccia decreased, outgassing would have been constrained to within the central portion of the conduit and promoted overpressure development, especially if the conduit diameter were to constrict (Castro et al. 2016) due to pyroclastic breccia emplacement at its walls. The gradual heating of the conduit walls during pyroclastic breccia emplacement would have eventually allowed fine-grained ash particles to stick to the conduit margins, allowing a transition to the formation of vitrophyre breccia (Fig. 12e).

The presence of the glassy contact within the pyroclastic breccia (Fig. 8) suggests that a sufficient temperature for welding at the conduit margins was reached before the start of vitrophyre breccia and vitrophyre formation. Whether the transition from pyroclastic breccia to vitrophyre breccia can occur will depend on multiple factors, such as the eruption explosivity and the grain size of material, where higher explosion intensity results in finer grain sizes (Kueppers et al. 2006; Fowler & Scheu 2016), thus facilitating more efficient welding. The shielding of the surrounding country rock by the pyroclastic breccia would reduce the number of lithics available, and the increased cohesion of the pyroclastic breccia would prevent overturning and reworking (Schipper et al. 2021). A drop in explosivity would also reduce the amount of quarrying that could occur, leaving a supply of ash-sized particles for vitrophyre breccia and vitrophyre formation that contained fewer lithic clasts (Fig. 12f). The vitrophyre breccia and vitrophyre were nearly entirely formed by the welding of ash-sized particles, with a few rare lithic clasts captured by the accreting material. Coherent vitrophyre, rather than vitrophyre breccia, would have been formed once the explosivity had dropped sufficiently to prevent the repeated fracturing of the accreting material.

Increased overpressure in the constricting conduit opened fractures that would become tuffisites within the vitrophyre and vitrophyre breccia, now acting as a passive and effectively static ‘country rock’. These tuffisites may have cross-cut only the vitrophyre or vitrophyre breccia, but given

greater overpressure the fractures may have propagated further to intersect the pyroclastic breccia or surrounding country rock (Fig. 12e).

Conduit sealing and the formation of the innermost vent units

Fine-grained, crystal-poor material that sticks to conduit margins can weld to form a dense glass (Gardner et al. 2017), preserved here as vitrophyre (Figs. 5c and 12e). The pressure-driven fracturing of this dense glassy vitrophyre produced the *in situ* jigsaw-fit clasts that form the vitrophyre breccia, separated by tuffisites. As the eruption waned further and erosive quarrying decreased, the accreting vitrophyre at the conduit margin was no longer fragmented and ejected, and merely damaged, until eventually that damage ceased. If the filling of the conduit were promoted by the welding of pyroclastic material and the entire silicic magma column were expected to be wholly fragmented at depth, the central conduit-plugging rhyolite lava would share a similar origin (Wadsworth et al. 2020). The continued accretion and welding of pyroclastic material would have eventually sealed part of or all of the vent, leading to the onset of welded-lava effusion to produce the flow-banded rhyolite lava at the vent center. A body of magma assembled at shallow depth could then be fractured to produce a network of permeable pathways along which pyroclastic material from below could be transported and deposited to form tuffisites (Wadsworth et al. 2020, 2022).

Discussion

Similarities between conduits and tuffisites

The initiation of an eruption can be considered as the continued propagation, expansion, and connection of tuffisites that evolve into a conduit. In the shallow subsurface (< 2-km depth) the silicic magma column is likely to be fragmented (Wadsworth et al. 2020). The deposition of clastic material within the conduit during the waning phase of an eruption means that preserved, dissected conduits will qualitatively resemble a tuffisite, as each is a pathway for pyroclastic discharge. The characteristics and overall structure of the MCV are remarkably similar to those of the tuffisites intersecting the vent units, albeit on a larger scale. Processes such as repeated erosion and deposition of material, injections, and welding, occur not only on a small scale within tuffisites but also on a much larger scale within the vent units (Schipper et al. 2021).

Once repeated injections of material into a tuffisite allow it to reach a sufficient thickness, the tuffisite centre becomes hot enough for welding and viscous deformation to occur

(Unwin et al. 2021). The same process at the conduit-scale will allow the pyroclastic breccia to weld and strengthen, changing the conduit pathway through time. Conduits are much larger than tuffisites and so will generally reach greater temperatures and cool more slowly, allowing more complete welding to occur (Kolzenburg et al. 2019). In a conduit where the margins have become sufficiently hot, ash particles can stick to and coat the conduit margins to form a vitrophyre unit (Gardner et al. 2017; Wadsworth et al. 2020). Similarly, sticking and coating of tuffisite vein walls by fine-grained ash can create dense veneers (Farquharson et al. 2022), which will have low permeability relative to the surrounding country rock (Wadsworth et al. 2022).

However, there are many important differences between tuffisites and conduits that control their evolution through time. While tuffisites are the initial stage of conduit evolution, the greater dimensions of a conduit allow for more mixing and overturn of material, preventing the formation and preservation of the complex internal structures seen within tuffisites (Valentine & Cole 2021). The shape of the vent is likely to create deposits that are more prone to slumping than within tuffisites, controlling the structure of the vent produced. The pressure gradients driving gas and particle flow within the conduit will likely be lower than within a tuffisite, due to the greater dimensions of the conduit, especially during waning activity, controlling the ability for pyroclasts to be re-entrained into the flow and for internal fracturing to occur (Unwin et al. 2021). The greater permeability of the conduit margin than tuffisite walls will also help to reduce the pressure gradient within the conduit by allowing for lateral gas escape (Heiken et al. 1988), lowering the flow velocity within the conduit. To inject material into a pre-existing host fracture to form a tuffisite, the fluid pressure must be great enough to displace the surrounding material (Unwin et al. 2021), while in a conduit continuous mixing, overturning and soft sediment deformation allows for the emplacement of new material at lower fluid pressures.

Flux through tuffisites during vent evolution

Tuffisites have been suggested to act ubiquitously as permeable pathways along which outgassing can occur, perhaps defusing gas pressure from a conduit (Farquharson et al. 2017; Kolzenburg et al. 2019). Therefore, tuffisite formation is thought to be key to understanding explosive-effusive transitions. By contrast, here, we show that the initial host-rock for ‘early’ tuffisites is a highly permeable vent-lining breccia (Online Resource 3) that would allow highly efficient outgassing (Eichelberger et al. 1986). ‘Early’ tuffisites in this host rock are not necessarily only hydrofracture driven and instead can also involve invasion of the pyroclastic debris with ash- and clast-laden fluids, which deposit as they percolate (White & Ross 2011). Such invasion could create

deposits that appear superficially tuffisitic, but actually sealed up outgassing routes in pre-existing deposits, without any initial high-permeability opening phase.

Once the conduit walls have been heated sufficiently for welding of fine material at the margins to form the vitrophyre and vitrophyre breccia, these lower permeability units (relative to the pyroclastic breccia) will seal the margins of the conduit, constraining fluid flow and increasing the fluid pressure within the active portion of the conduit. If a sufficient fluid pressure can be achieved to fracture the vitrophyre breccia, tuffisites can form a pathway through the less permeable material and into the more permeable pyroclastic breccia beyond, where outgassing can occur more effectively (Online Resource 3). Tuffisites therefore become necessary for lateral outgassing to occur in this partially or wholly sealed phase of the conduit evolution. Fracturing the dense vitrophyre breccia will require a greater fluid pressure than invading a pathway through the weaker, less compacted pyroclastic breccia, suggesting that once the vitrophyre unit begins to coat the conduit margins a higher fluid pressure can be achieved within the conduit. We propose that this corresponds to the formation of a dense lava plug, accompanied by repetitive Vulcanian explosions. If the dense glassy plug extends to the surface then hybrid activity could occur, as observed at Chaitén in 2008 (transitional phase 2; Pallister et al. 2013) and Cordón Caulle from June 15th 2011 (Schipper et al. 2013, 2021; Wadsworth et al. 2022).

Fine ash-sized particles, whether injected and deposited within a fracture or deposited within the pore space of coarser-grained material, will rapidly weld, sealing fluid flow pathways and reducing further outgassing. The permeability of these fluid pathways will therefore only be transient. The time-dependent porosity of a welding matrix with time, $\phi(t)$, can be estimated using the ‘vented bubble model’ (Wadsworth et al. 2019)

$$\frac{d\phi}{dt} = -\frac{3\Delta P}{4\mu}\phi - \frac{3\Gamma}{2\mu\langle a_i \rangle \zeta} \left(\frac{\phi_i}{1 - \phi_i} \right)^{\frac{1}{3}} \phi^{\frac{2}{3}}(1 - \phi)^{\frac{1}{3}} \quad (1)$$

where ϕ_i is the initial porosity, ΔP is the difference in pressure of the gas phase and stress acting on the particles involved in the welding, μ is the viscosity of the hot particles, Γ is the interfacial tension between the gas and the particle, and $\langle a_i \rangle$ is the mean size of the pore spaces between the welding particles (related to the particle size; Wadsworth et al. 2016). When $\Delta P \rightarrow 0$, Eq. (1) can be approximated by $\phi \approx \phi_i \exp(-3t/(2\lambda))$ where $\lambda = \zeta\mu \langle a_i \rangle / \Gamma$ is the welding timescale in the $\Delta P = 0$ regime (Wadsworth et al. 2014, 2016). Here, ζ is a correction factor that accounts for the polydispersivity of the particle size distribution (Wadsworth et al. 2017).

Referring to Eq. (1), $\Delta P \approx 0$ is justified for the case where the gas and particles are in pressure equilibrium (i.e., the

effective pressure is zero). At Mule Creek, this is likely to be the case in the conduit itself (i.e., during vitrophyre formation by welding) or in the early stages of tuffisite formation and welding. As tuffisites seal and gas pressure decays, there may be an increase in the pressure acting to compress the assemblage of particles relative to the gas pressure between the particles, causing ΔP to rise to $\Delta P > 0$, invalidating this simple approximation. Nevertheless, if we use the $\Delta P \approx 0$ assumption, we can give an upper-bound on λ . In order to compute λ , we must convert R_i to a_i and ζ . To do this, we use the model provided by Wadsworth et al. (2017), which, using the two distributions given in Fig. 10, yields $\langle a_i \rangle = 2.7 \times 10^{-7}$ m with $\zeta = 17.59$ (Fig. 10a) and $\langle a_i \rangle = 7.33 \times 10^{-6}$ m with $\zeta = 7.33$ (Fig. 10c), respectively. Using $\Gamma = 0.22$ N/m (Gardner & Ketcham, 2011), $5 \times 10^7 < \mu < 1.5 \times 10^9$ (using Hess & Dingwell, 1996; with a water content of 0.8 wt.% and for 700 and 800 °C from Stasiuk et al., 1996), we find that $18 < \lambda < 540$ min for the 2 μ m particles in the tuffisites within the pyroclastic breccia, or $37 < \lambda < 1107$ min for the 7 μ m particles in the tuffisites within the vitrophyre breccia. These timescales are far shorter than conduit cooling timescales (Kolzenburg et al. 2019), especially when thermally buffered by an ongoing bypassing eruption, with hot material flowing past the conduit walls, and well within the timescales associated with ongoing silicic eruptions (e.g. Schipper et al. 2013), lava assembly, and effusion (Wadsworth et al. 2020). This process will act more efficiently in early, high energy fragmentation events due to the correlation of grain size and fragmentation energy (Kueppers et al. 2006; Fowler & Scheu 2016) and slow down during the later waning stages of an eruption—further enhancing the discrepancy in the need for pressure release during the high energy stages and a more efficient outgassing and depressurization during later, waning phases.

The welding timescales in both cases explored here suggest that the welding material could efficiently lower the permeability of any outgassing pathways, potentially sealing them completely. In the pyroclastic breccia, welding of fine-grained intruded material could locally reduce the permeability, but with fluid flow pathways through the unconsolidated and permeable breccia relatively unconstrained, this reduction in permeability would likely not have a great effect on the bulk permeability of the unit. The accretion of the vitrophyre and vitrophyre breccia could quickly seal the conduit margins, rapidly decreasing their permeability. With gas unable to escape laterally through the impermeable vitrophyre and vitrophyre breccia, regular and repeated fracturing would be required to continually produce new lateral outgassing pathways to replace those sealed by welding.

As tuffisites close, gas pressure drops and ΔP will rise, and therefore, our estimate of the rate of porosity change is a conservative estimate (c.f. Eq. (1)). Similarly, if the gas pressure rises in tuffisites or between the welding

vitrophyre material, Eq. (1) predicts that ΔP will drop and can become negative, causing $d\phi/dt$ to be positive, and therefore porosity to increase with time as the gas pushes the sintering system apart again. Fractured masses of sintered particles within tuffisites in the vitrophyre breccia (Fig. 10d) suggest that this process does occur, perhaps due to the sealing or nearby permeable pathways locally increasing gas pressure (Unwin et al. 2021).

Future challenges

Tuffisite veins are pervasive throughout the width of the MCV, from the vitrophyre into the country rock, suggesting that they might play a role in influencing conduit dynamics throughout vent evolution. Characterization of the grain sizes, porosity, and permeability of tuffisites would determine how significant their role in outgassing might be, and whether tuffisites could carry a sufficient flux to defuse pressure within the evolving conduit. Further investigation of conduit walls would help constrain how their permeability and erodibility might vary through time, controlling the lateral outgassing flux through conduit walls and the conduit morphology throughout its evolution. This evolution of the permeability and erodibility of the conduit walls may also influence flow within the conduit, perhaps acting as a control on the steadiness of conduit flow through time. Detailed analysis of textures and H₂O contents across the margins of vents similar to Mule Creek may help to constrain degassing mechanisms. More closely integrating the spatial context provided by analysis at ancient dissected systems with the fragmental but fresh record preserved in pyroclasts from recent silicic eruptions is then needed to further improve our understanding of the processes controlling the explosive–effusive transition. Detailed textural analysis of the different clasts forming the vitrophyre breccia at Mule Creek and similar vents may also help to confirm whether this unit was brecciated in situ or formed of vitrophyre clasts fractured away from the vent margin and redeposited at a shallower depth. Similar structures to the those seen within the Mule Creek vent are seen in basaltic diatremes, and applying and adapting our understanding of vent formation to less silica-rich systems poses an additional challenge.

Conclusions

The structure of the Mule Creek vent is complex, with the characteristics of the different vent-filling units controlling its morphology during vent evolution. The pyroclastic breccia contains many erosive surfaces, reflecting the repeated deposition, erosion, and overturning

of pyroclastic material until sintering and compaction increased its cohesion and more stable conduit walls could form. Heating of the conduit walls and waning explosivity allowed the accretion of ash-sized particles to form the vitrophyre breccia unit, with glassy material repeatedly fractured and re-healed until explosivity waned sufficiently for a more coherent vitrophyre to accrete. The accretion and sintering of pyroclastic material eventually blocked the vent, leading to the eventual effusion of sintered lava and production of flow-banded rhyolite lava at the vent center.

The tuffisites that intersect every vent unit have complex internal structures, reflecting repeated periods of erosion and deposition within the fractures. Diffuse tuffisites in the pyroclastic breccia record lateral outgassing through the high permeability breccia lining the conduit margins. Repeated periods of erosion and deposition, driven by fluctuations in the conduit fluid pressure, caused the conduit width to vary through time. The accretion of ash-sized particles to form the vitrophyre and vitrophyre breccia would have effectively narrowed the active conduit, sealing the conduit margins and restricting lateral outgassing to the permeable pathways created by tuffisites.

Supplementary Information The online version contains supplementary material available at <https://doi.org/10.1007/s00445-023-01638-z>.

Acknowledgments We thank Leon Bowen for special assistance using the GJ Russell Electron Microscope Facility at Durham University and also Felix von Aulock for field assistance. We are grateful to the three reviewers and the editor for their constructive and insightful comments that have improved the manuscript.

Code availability This is not applicable.

Funding HU was supported by a NERC Envision studentship and a BUFI grant from the British Geological Survey. HT was supported by Royal Society URF 140716. Funding for AF was provided by a NERC PhD studentship from IAPETUS DTP.

Data availability All data and materials are available by request to the author.

Declarations

Conflict of interest The authors declare that the research was conducted in the absence of any commercial or financial relationships that could be construed as a potential conflict of interest.

Open Access This article is licensed under a Creative Commons Attribution 4.0 International License, which permits use, sharing, adaptation, distribution and reproduction in any medium or format, as long as you give appropriate credit to the original author(s) and the source, provide a link to the Creative Commons licence, and indicate if changes were made. The images or other third party material in this article are included in the article's Creative Commons licence, unless indicated otherwise in a credit line to the material. If material is not included in the article's Creative Commons licence and your intended use is not permitted by statutory regulation or exceeds the permitted use, you will need to obtain permission directly from the copyright holder. To view a copy of this licence, visit <http://creativecommons.org/licenses/by/4.0/>.

References

- Berlo K, Tuffen H, Smith VC et al (2013) Element variations in rhyolitic magma resulting from gas transport. *Geochim Cosmochim Acta* 121:436–451. <https://doi.org/10.1016/J.GCA.2013.07.032>
- Cabrera A, Weinberg RF, Wright HMN (2015) Magma fracturing and degassing associated with obsidian formation: the explosive–effusive transition. *J Volcanol Geotherm Res* 298:71–84. <https://doi.org/10.1016/J.JVOLGEORES.2014.12.014>
- Campbell ME, Russell JK, Porritt LA (2013) Thermomechanical milling of accessory lithics in volcanic conduits. *Earth Planet Sci Lett* 377–378:276–286. <https://doi.org/10.1016/J.EPSL.2013.07.008>
- Cassidy M, Manga M, Cashman K, Bachmann O (2018) Controls on explosive–effusive volcanic eruption styles. *Nat Commun* 9:2839. <https://doi.org/10.1038/s41467-018-05293-3>
- Castro JM, Bindeman I, Tuffen H, Schipper CI (2014) Explosive origin of silicic lava: textural and H₂O evidence for pyroclastic degassing during rhyolite effusion. *Earth Planet Sci Lett* 405:52–61
- Castro JM, Cordonnier B, Schipper CI et al (2016) Rapid laccolith intrusion driven by explosive volcanic eruption. *Nat Commun* 7:13585. <https://doi.org/10.1038/ncomms13585>
- Castro JM, Cordonnier B, Tuffen H et al (2012) The role of melt-fracture degassing in defusing explosive rhyolite eruptions at volcán Chaitén. *Earth Planet Sci Lett* 333–334:63–69. <https://doi.org/10.1016/J.EPSL.2012.04.024>
- Castro JM, Dingwell DB (2009) Rapid ascent of rhyolitic magma at Chaitén volcano, Chile. *Nature* 461:780–783. <https://doi.org/10.1038/nature08458>
- Cataldo E, Davies AG, Wilson L (2013) Near-vertical supersonic and shock-free gas/magma flow at Ionian volcanoes: application to Pillan. *Icarus* 226:1171–1176. <https://doi.org/10.1016/J.ICARUS.2013.06.035>
- Cloos H (1941) Bau und taetigkeit von tuffschloten; Untersuchungen an dem schwaebischen vulkan. *Geol Rundsch* 32:709–800. <https://doi.org/10.1007/BF01801913>
- Cosgrove JW (2001) Hydraulic fracturing during the formation and deformation of a basin: a factor in the dewatering of low-permeability sediments. *AAPG Bulletin* 85(4):737–748
- Eichelberger JC, Carrigan CR, Westrich HR, Price RH (1986) Non-explosive silicic volcanism. *Nature* 323(6089):598–602. <https://doi.org/10.1038/323598a0>
- Farquharson J, Heap MJ, Varley NR et al (2015) Permeability and porosity relationships of edifice-forming andesites: a combined field and laboratory study. *J Volcanol Geotherm Res* 297:52–68. <https://doi.org/10.1016/j.jvolgeores.2015.03.016>
- Farquharson J, Tuffen H, Wadsworth F et al (2022) In-conduit capture of sub-micron volcanic ash particles via turbophoresis and sintering. *Nat Commun* 13(1):4713. <https://doi.org/10.21203/rs.3.rs-1152244/v1>
- Farquharson JI, Wadsworth FB, Heap MJ, Baud P (2017) Time-dependent permeability evolution in compacting volcanic fracture systems and implications for gas overpressure. *J Volcanol Geotherm Res* 339:81–97. <https://doi.org/10.1016/J.JVOLGEORES.2017.04.025>
- Fowler AC, Scheu B (2016) A theoretical explanation of grain size distributions in explosive rock fragmentation. *Proc R Soc A: Math Phys En* 472(2190):20150843. <https://doi.org/10.1098/RSPA.2015.0843>
- Gardner JE, Ketcham RA (2011) Bubble nucleation in rhyolite and dacite melts: temperature dependence of surface tension. *Contrib Mineral Petrol* 162:929–943. <https://doi.org/10.1007/S00410-011-0632-5/FIGURES/7>
- Gardner JE, Llewellyn EW, Watkins JM, Befus KS (2017) Formation of obsidian pyroclasts by sintering of ash particles in the volcanic conduit. *Earth Planet Sci Lett* 459:252–263. <https://doi.org/10.1016/j.epsl.2016.11.037>
- Gardner JE, Wadsworth FB, Llewellyn EW et al (2018) Experimental sintering of ash at conduit conditions and implications for the longevity of tuffisites. *Bull Volcanol* 80:1–14. <https://doi.org/10.1007/s00445-018-1202-8>
- Gardner JE, Wadsworth FB, Llewellyn EW et al (2019) Experimental constraints on the textures and origin of obsidian pyroclasts. *Bull Volcanol* 81:1–15. <https://doi.org/10.1007/S00445-019-1283-Z/FIGURES/10>
- Gaunt EH, Sammonds PR, Meredith PGP et al (2014) Pathways for degassing during the lava dome eruption of Mount St. Helens 2004–2008. *Geology* 42:947–950. <https://doi.org/10.1130/G35940.1>
- Giachetti T, Trafton KR, Wiejaczka J et al (2021) The products of primary magma fragmentation finally revealed by pumice agglomerates. *Geology* 49(11):1307–1311. <https://doi.org/10.1130/G48902.1>
- Gonnermann HM, Manga M (2003) Explosive volcanism may not be an inevitable consequence of magma fragmentation. *Nature* 426:432–435. <https://doi.org/10.1038/nature02138>
- Goto Y, Nakada S, Kurokawa M et al (2008) Character and origin of lithofacies in the conduit of Unzen volcano, Japan. *J Volcanol Geotherm Res* 175:45–59. <https://doi.org/10.1016/J.JVOLGEORES.2008.03.041>
- Heap MJ, Tuffen H, Wadsworth FB et al (2019) The permeability evolution of tuffisites and implications for outgassing through dense rhyolitic magma. *J Geophys Res Solid Earth* 124:8281–8299. <https://doi.org/10.1029/2018JB017035>
- Heiken G, Wohletz K, Eichelberger J (1988) Fracture fillings and intrusive pyroclasts, Inyo Domes, California. *J Geophys Res Solid Earth* 93:4335–4350. <https://doi.org/10.1029/JB093iB05p04335>
- Hess K-U, Dingwell DD (1996) Viscosities of hydrous leucogranitic melts: a non-Arrhenian model. *Am Mineral* 81:1297–1300. <https://doi.org/10.2138/AM-1996-9-1031>
- Jaupart C (1998) Gas loss from magmas through conduit walls during eruption. *Geol Soc Spec Pub* 145:73–90. <https://doi.org/10.1144/GSL.SP.1996.145.01.05>
- Jaupart C, Allègre CJ (1991) Gas content, eruption rate and instabilities of eruption regime in silicic volcanoes. *Earth Planet Sci Lett* 102:413–429. [https://doi.org/10.1016/0012-821X\(91\)90032-D](https://doi.org/10.1016/0012-821X(91)90032-D)
- Kendrick JE, Lavallée Y, Varley NR et al (2016) Blowing off steam: tuffisite formation as a regulator for lava dome eruptions. *Front Earth Sci* 4:41. <https://doi.org/10.3389/feart.2016.00041>
- Kolzenburg S, Russell JK (2014) Welding of pyroclastic conduit infill: a mechanism for cyclical explosive eruptions. *J Geophys Res Solid Earth* 119:5305–5323. <https://doi.org/10.1002/2013JB010931>
- Kolzenburg S, Ryan AG, Russell JK (2019) Permeability evolution during non-isothermal compaction in volcanic conduits and tuffisite veins: implications for pressure monitoring of volcanic edifices. *Earth Planet Sci Lett* 527:115783. <https://doi.org/10.1016/j.epsl.2019.115783>
- Kueppers U, Perugini D, Dingwell DB (2006) “Explosive energy” during volcanic eruptions from fractal analysis of pyroclasts. *Earth Planet Sci Lett* 248:800–807. <https://doi.org/10.1016/J.EPSL.2006.06.033>
- Lara LE (2009) The 2008 eruption of Chaitén volcano, Chile: a preliminary report. *Andean Geology* 36:125–129
- Lavallée Y, Benson PM, Heap MJ et al (2013) Reconstructing magma failure and the degassing network of dome-building eruptions. *Geology* 41:515–518. <https://doi.org/10.1130/G33948.1>
- Lormand C, Zellmer GF, Németh K et al (2018) Weka trainable segmentation plugin in ImageJ: a semi-automatic tool applied to

- crystal size distributions of microlites in volcanic rocks. *Microsc Microanal* 24:667–675. <https://doi.org/10.1017/S1431927618015428>
- McGowan EM (2016) Magma emplacement and deformation in rhyolitic dykes : insight into magmatic outgassing. PhD thesis., University of Lancaster
- Paisley R, Berlo K, Ghaleb B, Tuffen H (2019) Geochemical constraints on the role of tuffisite veins in degassing at the 2008–09 Chaitén and 2011–12 Cordón Caulle rhyolite eruptions. *J Volcanol Geotherm Res* 380:80–93. <https://doi.org/10.1016/j.jvolgeores.2019.05.013>
- Pallister JS, Cashman KV, Hagstrum JT et al (2013) Faulting within the Mount St. Helens conduit and implications for volcanic earthquakes. *Bull Geol Soc Am* 125:359–376. <https://doi.org/10.1130/B30716.1>
- Perkins TK, Kern LR (1961) Widths of hydraulic fractures. *J Petrol Tech* 13:937–949. <https://doi.org/10.2118/89-PA>
- Phillips E, Everest J, Reeves H (2013) Micromorphological evidence for subglacial multiphase sedimentation and deformation during overpressurized fluid flow associated with hydrofracturing. *Boreas* 42:395–427. <https://doi.org/10.1111/j.1502-3885.2012.00261.x>
- Ratté JC (2004) A guide to the Mule Creek volcanic vent, the rhyolite of Potholes Country, and obsidian ledges, Gila National Forest, southwestern New Mexico. *New Mexico Geology* 26:111–122
- Ross PS, Carrasco Núñez G, Hayman P (2017) Felsic maar-diatreme volcanoes: a review. *Bull Volcanol* 79:1–33. <https://doi.org/10.1007/s00445-016-1097-1>
- Ross PS, White JDL (2006) Debris jets in continental phreatomagmatic volcanoes: a field study of their subterranean deposits in the Coombs Hills vent complex, Antarctica. *J Volcanol Geotherm Res* 149:62–84. <https://doi.org/10.1016/j.jvolgeores.2005.06.007>
- Rust AC, Cashman KV, Wallace PJ (2004) Magma degassing buffered by vapor flow through brecciated conduit margins. *Geology* 32:349. <https://doi.org/10.1130/G20388.2>
- Saubin E, Tuffen H, Gurioli L et al (2016) Conduit dynamics in transitional rhyolitic activity recorded by tuffisite vein textures from the 2008–2009 Chaitén eruption. *Front Earth Sci* 4:59. <https://doi.org/10.3389/feart.2016.00059>
- Schipper CI, Castro JM, Kennedy BM et al (2021) Silicic conduits as supersized tuffisites: clastogenic influences on shifting eruption styles at Cordón Caulle volcano (Chile). *Bull Volcanol* 83:1–22. <https://doi.org/10.1007/s00445-020-01432-1>
- Schipper CI, Castro JM, Tuffen H et al (2013) Shallow vent architecture during hybrid explosive–effusive activity at Cordón Caulle (Chile, 2011–12): evidence from direct observations and pyroclast textures. *J Volcanol Geotherm Res* 262:25–37. <https://doi.org/10.1016/J.JVOLGEORES.2013.06.005>
- Schipper CI, Castro JM, Tuffen H et al (2015) Cristobalite in the 2011–2012 Cordón Caulle eruption (Chile). *Bull Volcanol* 77:1–19. <https://doi.org/10.1007/S00445-015-0925-Z/FIGURES/7>
- Schneider CA, Rasband WS, Eliceiri KW (2012) NIH Image to ImageJ: 25 years of image analysis. *Nat Methods* 9(7):671–675. <https://doi.org/10.1038/nmeth.2089>
- SERNAGEOMIN-OVDAS (2011) Puyehue-Cordón Caulle: reporte especial de actividad volcánica. Internal report 38. SERNAGEOMIN-OVDAS, Arica, Chile
- Shea T, Houghton B, Gurioli L et al (2010) Textural studies of vesicles in volcanic rocks: an integrated methodology. *J Volcanol Geotherm Res* 190(3–4):271–289. <https://doi.org/10.1016/j.jvolgeores.2009.12.003>
- Stasiuk M, Barclay J, Carroll MR et al (1996) Degassing during magma ascent in the Mule Creek vent (USA). *Bull Volcanol* 58:117–130. <https://doi.org/10.1007/s004450050130>
- Tuffen H, Dingwell D (2005) Fault textures in volcanic conduits: evidence for seismic trigger mechanisms during silicic eruptions. *Bull Volcanol* 67:370–387. <https://doi.org/10.1007/s00445-004-0383-5>
- Tuffen H, Dingwell DB, Pinkerton H (2003) Repeated fracture and healing of silicic magma generate flow banding and earthquakes? *Geology* 31:1089. <https://doi.org/10.1130/G19777.1>
- Unwin HE, Tuffen H, Phillips E et al (2021) Pressure-driven opening and filling of a volcanic hydrofracture recorded by tuffisite at Húsafell, Iceland: a potential seismic source. *Front Earth Sci* 9:347. <https://doi.org/10.3389/feart.2021.668058>
- Valentine GA, Cole MA (2021) Explosive caldera-forming eruptions and debris-filled vents: gargle dynamics. *Geology* 49:1240–1244. <https://doi.org/10.1130/G48995.1>
- Valentine GA, White JDL (2012) Revised conceptual model for maar-diatremes: subsurface processes, energetics, and eruptive products. *Geology* 40:1111–1114. <https://doi.org/10.1130/G33411.1>
- Wadsworth FB, Vasseur J, Scheu B et al (2016) Universal scaling of fluid permeability during volcanic welding and sediment diagenesis. *Geology* 44:219–222. <https://doi.org/10.1130/G37559.1>
- Wadsworth FB, Vasseur J, Llewellyn EW et al (2017) Sintering of poly-disperse viscous droplets. *Phys Rev E* 95(3). <https://doi.org/10.1103/PhysRevE.95.033114>
- Wadsworth FB, Witcher T, Vossen CEJ et al (2018) Combined effusive-explosive silicic volcanism straddles the multiphase viscous-to-brittle transition. *Nat Commun* 9:1–8. <https://doi.org/10.1038/s41467-018-07187-w>
- Wadsworth FB, Vasseur J, Schaubroth J et al (2019) A general model for welding of ash particles in volcanic systems validated using in situ X-ray tomography. *Earth Planet Sci Lett* 525:115726. <https://doi.org/10.1016/j.epsl.2019.115726>
- Wadsworth FB, Llewellyn EW, Vasseur J et al (2020) Explosive-effusive volcanic eruption transitions caused by sintering. *Sci Adv* 6(39). <https://doi.org/10.1126/sciadv.aba7940>
- Wadsworth FB, Vasseur J, Llewellyn EW et al (2021) A model for permeability evolution during volcanic welding. *J Volcanol Geotherm Res* 409:107118. <https://doi.org/10.1016/J.JVOLGEORES.2020.107118>
- Wadsworth FB, Llewellyn EW, Castro JM et al (2022) A reappraisal of explosive–effusive silicic eruption dynamics: syn-eruptive assembly of lava from the products of cryptic fragmentation. *J Volcanol Geotherm Res* 432:107672. <https://doi.org/10.1016/J.JVOLGEORES.2022.107672>
- Wadsworth FB, Vasseur J, von Aulock FW et al (2014) Nonisothermal viscous sintering of volcanic ash. *J Geophys Res Solid Earth* 119:8792–8804. <https://doi.org/10.1002/2014JB011453>
- White JDL, Ross PS (2011) Maar-diatreme volcanoes: a review. *J Volcanol Geotherm Res* 201:1–29. <https://doi.org/10.1016/J.JVOLGEORES.2011.01.010>
- Wilson L, Head JW (1981) Ascent and eruption of basaltic magma on the Earth and Moon. *J Geophys Res Solid Earth* 86:2971–3001. <https://doi.org/10.1029/JB086iB04p02971>

In the Supplementary Information, we provide two animations of the proposed evolution captured in our conceptual model (Fig. 12). EP publishes with the permission of the Executive Director of the British Geological Survey.